

# Single-Shot Decoding and Fault-tolerant Gates with Trivariate Tricycle Codes

Abraham Jacob,<sup>1,\*</sup> Campbell McLaughlan,<sup>1,2,\*</sup> and Dan E. Browne<sup>1</sup>

<sup>1</sup>*Department of Physics & Astronomy, University College London, London, WC1E 6BT, United Kingdom*

<sup>2</sup>*Centre for Engineered Quantum Systems, School of Physics,  
University of Sydney, Sydney, NSW 2006, Australia*

While quantum low-density parity check (qLDPC) codes are a low-overhead means of quantum information storage, it is valuable for quantum codes to possess fault-tolerant features beyond this resource efficiency. In this work, we introduce trivariate tricycle (TT) codes, qLDPC codes that combine several desirable features: high thresholds under a circuit-level noise model, partial single-shot decodability for low-time-overhead decoding, a large set of transversal Clifford gates and automorphisms within and between code blocks, and (for several sub-constructions) constant-depth implementations of a (non-Clifford)  $CCZ$  gate. TT codes are CSS codes based on a length-3 chain complex, and are defined from three trivariate polynomials, with the 3D toric code (3DTC) belonging to this construction. We numerically search for TT codes and find several candidates with improved parameters relative to the 3DTC, using up to  $48\times$  fewer data qubits as equivalent 3DTC encodings. We construct syndrome-extraction circuits for these codes and numerically demonstrate single-shot decoding in the  $X$  error channel in both phenomenological and circuit-level noise models. Under circuit-level noise, TT codes have a threshold of 0.3% in the  $Z$  error channel and 1% in the  $X$  error channel (with single-shot decoding). All TT codes possess several transversal  $CZ$  gates that can partially address logical qubits between two code blocks. Additionally, the codes possess a large set of automorphisms that can perform Clifford gates within a code block. Finally, we establish several TT code polynomial constructions that allows for a constant-depth implementation of logical  $CCZ$  gates. We find examples of error-correcting and error-detecting codes using these constructions whose parameters out-perform those of the 3DTC, using up to  $4\times$  fewer data qubits for equivalent-distance 3DTC encodings.

## I. INTRODUCTION

Quantum error-correction (QEC) is a necessary feature of any large-scale quantum computing architecture. The surface code [1–4] is a very promising candidate QEC code, with mature fault-tolerant schemes for performing logic on encoded qubits [5], including lattice surgery [6], low overhead measurements in all bases [7], and twist and hole braiding [8]. However, even with recent theoretical results on resource savings with the surface code [9, 10], the very large resource estimates for achieving useful quantum advantage [11] mean that we should consider the use of higher-rate quantum low-density parity check (qLDPC) codes.

The bivariate bicycle (BB) codes [12] are a class of code with very good encoding rates and relative distances. They perform well under a circuit-level noise model, exhibiting high thresholds comparable to the surface code. As such, they are a promising candidate for a qLDPC code that can help lower the overheads of fault-tolerant quantum computing [13]. There has been a great deal of investigation into the the classes to which these codes belong, with the aim of finding codes with improved parameters and properties [14–19], and implementing them in hardware [20, 21].

Meanwhile, there has been interest in developing codes that display other useful features. To address the large time overheads and associated classical compute re-

sources required for decoding qLDPC codes [11], much effort has gone into finding codes with single-shot decodability [22–26] and other single-shot properties [27, 28]. Single-shot codes can allow for decoding to be performed on small amounts of syndrome data, collected over a constant number of QEC cycles, without incurring a significant drop in accuracy. The presence of meta-checks, which help determine when syndrome measurement errors have been made, can assist with this type of strategy, as well as allowing for operations such as lattice surgery to be performed with constant time-overhead [28].

A large set of transversal gates and automorphisms is useful for fault-tolerant computing with qLDPC codes, and recent work has focused on finding codes with (fold-)transversal Clifford gates [29–33], automorphisms [12, 34], and low-depth non-Clifford gates [35–38]. The former two provide logical primitives that can speed up an array of fault-tolerant computing schemes [32], even those based on Pauli-based computation (involving the measurement of high-weight logical operators within and between code blocks) [13, 39]. The latter can provide new avenues towards low-overhead magic-state preparation [40] and distillation [41].

Despite this recent intense activity, a thorough investigation of codes that *combine* several of these desirable properties has been lacking. To that end we introduce the trivariate tricycle (TT) codes, generalisations of the BB codes, that exhibit several useful features. These codes are based on a length-3 chain complex and hence possess meta-checks for one of the bases, which we take to be the  $Z$  check basis. We introduce a quantity which we call “meta-check distance”, useful for considerations

\* These authors contributed equally.

such as generalised lattice surgery [28], and show that it is equal to the  $Z$ -distance of the code. The 3D toric code (3DTC) belongs to this code family, and indeed, we can lay out the TT codes on a cubic lattice without boundary, with additional long-range connections. We numerically find several medium-size examples of TT codes that exhibit parameters that far exceed those of the surface code and 3DTC, for an equivalent number of logical qubits and code distance. All TT codes found have large  $X$  distances, with  $d_X > d_Z$ , which could be useful for architectures with biased noise qubits [42]. We identify a minimum-depth syndrome measurement circuit for the TT codes and numerically evaluate the codes' performance under phenomenological noise and circuit-level noise, finding that TT codes possess high thresholds despite the large check weights. We evaluate the single-shot performance of the codes (under both noise models) using an overlapping window strategy [25], numerically observing that  $Z$  memory experiment performance displays evidence of single-shot decodability.

We find that several logical  $\overline{CZ}$  gates can be performed transversally on the  $TT$  code logical qubits between two blocks of code, while shift automorphisms can perform certain Clifford gates within a code block. Up to in-block automorphisms, there are three non-equivalent logical  $\overline{CZ}$  gates. For many of the TT codes we discuss, the logical qubits can be divided into one of three sets. Two of the three logical  $\overline{CZ}$  gates have a simple form on these logical sets, preserving one and entangling the other two.

Finally, we introduce several TT code constructions that allow a constant-depth circuit of  $CCZ$  gates to preserve the code space. We thereby find codes with non-Clifford gates whose parameters greatly outperform those of the 3DTC. As an example, our  $[[48, 3, 4]]$  code with  $Z$ -distance 4 and  $X$ -distance 8 uses 1/4 of the data qubits of the regular 3DTC (with  $Z$ -distance 4). We find codes with better encoding rates that also admit non-trivial  $\overline{CCZ}$  gates, but which seem to be limited to have  $Z$ -distance 2 for one or more of the logical qubits. They are thus error-correcting in one basis ( $d_X > 2$ ) but only error-detecting in the other ( $d_Z = 2$ ). By gauge-fixing one or more logical qubits in these distance-2 codes, we can obtain error-correcting codes ( $d \geq 3$ ) with an additional  $CZ$  gate implementable between two code blocks.

This paper is structured as follows. In Section II, we introduce the code construction and prove several important Lemmas relating to the code parameters and code equivalences. We also introduce a layout for these codes on a 3D cubic grid with additional long-range connections. Section III investigates the performance of TT codes under phenomenological noise, showing evidence of a threshold for small-to-medium instances of TT codes in memory experiments. In Section IV we present circuit-level noise simulations of TT code performance, demonstrating evidence for thresholds in both  $X$  and  $Z$  memory experiments and single-shot capabilities for  $Z$  memory using an overlapping window decoding method. In Section V, we introduce the decomposition of logical qubits

into the three logical sets, along with the shift automorphisms and transversal  $CZ$  gates that are possible in any TT code. We then discuss the sub-constructions that allow for constant-depth  $CCZ$  circuits to be defined. We prove that a large class of such constructions exist, and present codes with logical  $\overline{CCZ}$  gates found through exhaustive searches over small code sizes. In Section VI we conclude and present several directions for future work. In the Appendices, we present further examples of TT codes found through random search, prove that our syndrome measurement circuits function as claimed, and provide further details on methods relating to codes with constant-depth  $CCZ$  circuits.

## II. 3-BLOCK AND TRIVARIATE TRICYCLE CODES

We first define arbitrary 3-block group algebra codes (for Abelian group  $G$ ), before introducing the trivariate tricycle codes more explicitly. For a general introduction on group algebra code constructions, see Ref. [17]. We will be considering the group algebra  $\mathbb{F}_2[G]$ , consisting of formal sums of the form  $\sum_{g \in G} a_g g$ , with  $a_g \in \mathbb{F}_2$ . The sum and product of two elements from  $\mathbb{F}_2[G]$  are defined in the natural way. For a 3-block code, we introduce three length-1 chain complexes –  $\mathcal{A}_1 \xrightarrow{a} \mathcal{A}_0$ ,  $\mathcal{B}_1 \xrightarrow{b} \mathcal{B}_0$ , and  $\mathcal{C}_1 \xrightarrow{c} \mathcal{C}_0$  – where  $\mathcal{A}_i, \mathcal{B}_i, \mathcal{C}_i = \mathbb{F}_2[G]$  and  $a, b, c \in \mathbb{F}_2[G]$ . We will then be considering the tensor/balanced product complex formed from these three length-1 complexes. For general treatments of balanced products, see Refs. [35, 43, 44]. We need not define the tensor product of  $\mathbb{F}_2[G]$ -modules in general, since we can simply note that  $\mathbb{F}_2[G] \otimes_G \mathbb{F}_2[G] \simeq \mathbb{F}_2[G]$ . The tensor product complex is then:

$$\mathcal{A}_1 \otimes_G \mathcal{B}_1 \otimes_G \mathcal{C}_1 \xrightarrow{\partial_3} \bigoplus_{i+j+k=2} \mathcal{A}_i \otimes_G \mathcal{B}_j \otimes_G \mathcal{C}_k \xrightarrow{\partial_2} \bigoplus_{i+j+k=1} \mathcal{A}_i \otimes_G \mathcal{B}_j \otimes_G \mathcal{C}_k \xrightarrow{\partial_1} \mathcal{A}_0 \otimes_G \mathcal{B}_0 \otimes_G \mathcal{C}_0. \quad (1)$$

The boundary maps can be written in terms of  $a$ ,  $b$ , and  $c$  as:

$$\partial_3 = \begin{bmatrix} a \\ b \\ c \end{bmatrix} \quad (2)$$

$$\partial_2 = \begin{bmatrix} 0 & c & b \\ c & 0 & a \\ b & a & 0 \end{bmatrix} \quad (3)$$

$$\partial_1 = [a \ b \ c]. \quad (4)$$

We will now construct the trivariate tricycle codes from this abstract chain complex. We first set  $G = \mathbb{Z}_\ell \times \mathbb{Z}_m \times \mathbb{Z}_p$ , for integers  $\ell, m$ , and  $p$ . Define the following matrices

which together generate this group:

$$x = S_\ell \otimes \mathbb{1}_m \otimes \mathbb{1}_p, \quad (5)$$

$$y = \mathbb{1}_\ell \otimes S_m \otimes \mathbb{1}_p, \quad (6)$$

$$z = \mathbb{1}_\ell \otimes \mathbb{1}_m \otimes S_p, \quad (7)$$

where  $S_\ell$  is the cyclic shift matrix, whose elements are  $\delta_{i,i\oplus 1}$ , where  $\oplus$  here refers to addition mod  $\ell$ . We then introduce matrices  $A$ ,  $B$  and  $C$ , which will be polynomials in these three variables. These will take the positions of  $a$ ,  $b$ , and  $c$  in Equations 2–4. For now, we will consider each polynomial to contain three terms:

$$A = A_1 + A_2 + A_3 \quad (8)$$

$$B = B_1 + B_2 + B_3 \quad (9)$$

$$C = C_1 + C_2 + C_3 \quad (10)$$

though we will later relax this restriction. We then let  $H_X \equiv \partial_1$ ,  $H_Z = \partial_2^\top$  and  $M_Z = \partial_3^\top$ , where  $H_X$  and  $H_Z$  represent the usual parity check matrices of a CSS code, and  $M_Z$  is a matrix of *meta-checks*, encoding the redundancy in the  $Z$  checks. It can be verified that  $H_X H_Z^\top = M_Z H_Z = 0$ . To summarise, this results in the following chain complex structure:

$$\mathcal{C}_M \xleftarrow{M_Z} \mathcal{C}_Z \xleftarrow{H_Z} \mathcal{Q} \xrightarrow{H_X} \mathcal{C}_X \quad (11)$$

with all spaces defined as vector spaces over  $\mathbb{F}_2$ :  $\mathcal{Q}, \mathcal{C}_X, \mathcal{C}_Z$ , and  $\mathcal{C}_M$  correspond to qubits,  $X$ -checks,  $Z$ -checks and  $Z$ -meta-checks, respectively. The matrices are given by:

$$M_Z = [A^\top \ B^\top \ C^\top] \quad (12)$$

$$H_Z = \begin{bmatrix} 0 & C^\top & B^\top \\ C^\top & 0 & A^\top \\ B^\top & A^\top & 0 \end{bmatrix} \quad (13)$$

$$H_X = [A \ B \ C]. \quad (14)$$

### A. Code parameters and explicit examples

Here, we discuss the parameters of and equivalences among TT codes, before introducing explicit examples. A trivariate tricycle (TT) code is defined on  $n = 3\ell m p$  data qubits. We begin by discussing the number of logical qubits. We have:

**Lemma 1.** *For a TT code with  $H_Z$  and  $H_X$  defined in Equations 13 and 14, respectively, the number of logical qubits is given by:*

$$k = -\frac{n}{3} + \dim(\ker A \cap \ker B \cap \ker C) + \dim(\ker[0 \ C \ B] \cap \ker[C \ 0 \ A] \cap \ker[B \ A \ 0]). \quad (15)$$

*Proof.* As usual for a CSS code,  $k = n - \text{rk}(H_X) - \text{rk}(H_Z)$ , where we use  $\text{rk}(M)$  to refer to the rank of matrix  $M$ .

Now note that:

$$\text{rk}(H_X) = \frac{n}{3} - \dim(\ker H_X^\top). \quad (16)$$

Let  $\bar{C}_\ell$  be the  $\ell \times \ell$  permutation matrix with elements  $\delta_{-i,i}$ , where the minus is taken mod  $\ell$ . This has the property that  $\bar{C} S_\ell \bar{C} = S_\ell^\top$ . Similarly define  $\bar{C}_m$  and  $\bar{C}_p$ , and let  $\bar{C} = \bar{C}_\ell \otimes \bar{C}_m \otimes \bar{C}_p$ . Then we have:

$$H_X^\top = \begin{bmatrix} A^\top \\ B^\top \\ C^\top \end{bmatrix} = \begin{bmatrix} \bar{C} & 0 & 0 \\ 0 & \bar{C} & 0 \\ 0 & 0 & \bar{C} \end{bmatrix} \begin{bmatrix} A \\ B \\ C \end{bmatrix} \bar{C}. \quad (17)$$

Hence,  $H_X^\top$  differs from  $[A^\top \ B^\top \ C^\top]^\top$  by multiplication on the left and right by invertible matrices (since  $\bar{C}$  is self-inverse). Therefore, the dimensions of their kernels are equivalent. Finally,

$$\dim \left( \ker \begin{bmatrix} A \\ B \\ C \end{bmatrix} \right) = \dim(\ker A \cap \ker B \cap \ker C). \quad (18)$$

Similarly, we can see that  $\text{rk}(H_Z) = \text{rk}(H_Z^\top) = n - \dim(\ker[0 \ C \ B] \cap \ker[C \ 0 \ A] \cap \ker[B \ A \ 0])$ .  $\square$

The code distances  $d_X$  and  $d_Z$  are defined as:

$$d_X = \min\{|v| : v \in \ker(H_Z) \setminus \text{rs}(H_X)\} \quad (19)$$

$$d_Z = \min\{|v| : v \in \ker(H_X) \setminus \text{rs}(H_Z)\} \quad (20)$$

where  $\text{rs}(M)$  denotes the row space of matrix  $M$ . In TT codes,  $d_X \neq d_Z$  in general, and we observe that in all cases tested,  $d_X \geq d_Z$ . We can also introduce a quantity we call the *meta-check distance* similarly:

$$d_M = \min\{|v| : v \in \ker(M_Z) \setminus \text{cs}(H_Z)\} \quad (21)$$

where  $\text{cs}(M)$  denotes the column space of  $M$ . Because the meta-checks encode redundancies in the  $Z$ -checks, they can be used to repair faulty syndromes resulting from classical measurement errors. The interpretation of the meta-check distance is that it is the minimum number of classical measurement errors that can be made when measuring the  $Z$ -checks without triggering any meta-checks. A large meta-check distance ensures good performance under single-shot decoding, since we are likely to repair the syndrome accurately. A large meta-check distance also allows for a reduced time-overhead during logical operations like lattice surgery [28]. We have the following:

**Lemma 2.** *For a TT code defined as above,  $d_M = d_Z$ , and  $d_X = \min\{|v| : v \in \ker(H_Z^\top) \setminus \text{rs}(M_Z)\}$ .*

*Proof.* Suppose that  $v$  is a minimum-weight “check logical”, that is, it is in  $\ker(M_Z) \setminus \text{cs}(H_Z)$ . Let  $v =$

$[[\mathbf{n}, \mathbf{k}, \mathbf{d}]]$	Encoding Rate $\mathbf{r}$	$\ell, \mathbf{m}, \mathbf{p}$	$\mathbf{A}$	$\mathbf{B}$	$\mathbf{C}$	$d_X$	$d_Z$
$[[72, 6, 6]]$	1/12	4, 3, 2	$1 + y + xy^2$	$1 + yz + x^2y^2$	$1 + xy^2z + x^2y$	12	6
$[[180, 12, 8]]$	1/15	5, 4, 3	$1 + x^2y^3z + x^4y$	$1 + x^3 + x^4z^2$	$1 + x^3y^3 + x^4yz^2$	20	8
$[[432, 12, 12]]$	1/36	6, 6, 4	$1 + xyz^3 + x^3y^4z^2$	$1 + x^3yz^2 + x^3y^2z^3$	$1 + x^4y^3z^3 + x^5z^2$	$\leq 36$	12

TABLE I. Example trivariate tricycle codes and their parameters, along with the polynomials  $A$ ,  $B$  and  $C$  that define them. We report the encoding rates  $r = k/n$  along with the  $Z$  and  $X$  distances, which are inequivalent for TT codes.

$[\alpha^\top \beta^\top \gamma^\top]^\top$ . Then define the following:

$$\bar{v} = \begin{bmatrix} \bar{C}\alpha \\ \bar{C}\beta \\ \bar{C}\gamma \end{bmatrix}. \quad (22)$$

This vector is in the kernel of  $H_X$ , since:

$$H_X \bar{v} = [A \ B \ C] \begin{bmatrix} \bar{C}\alpha \\ \bar{C}\beta \\ \bar{C}\gamma \end{bmatrix} = \bar{C}(A^\top \alpha + B^\top \beta + C^\top \gamma) = 0. \quad (23)$$

Therefore  $\bar{v}$  is a logical operator unless it belongs to the row space of  $H_Z$ . In this case,  $\bar{v} = H_Z^\top w$ , for some vector  $w$ . But then:

$$\begin{bmatrix} \bar{C} & 0 & 0 \\ 0 & \bar{C} & 0 \\ 0 & 0 & \bar{C} \end{bmatrix} v = H_Z^\top w \implies v = \begin{bmatrix} \bar{C} & 0 & 0 \\ 0 & \bar{C} & 0 \\ 0 & 0 & \bar{C} \end{bmatrix} H_Z^\top w \quad (24)$$

$$= H_Z \begin{bmatrix} \bar{C} & 0 & 0 \\ 0 & \bar{C} & 0 \\ 0 & 0 & \bar{C} \end{bmatrix} w, \quad (25)$$

and so  $v \in \text{cs}(H_Z)$ , which contradicts the assumption that it was a check logical. Hence,  $\bar{v}$  is a logical  $Z$  operator. It has the same weight as  $v$  since  $\bar{C}$  does not change the weight of the vectors  $\alpha$ ,  $\beta$  and  $\gamma$ . Since we assumed that  $v$  was a minimum-weight check logical, we see that  $d_Z \leq d_M$ . One can, in exactly the same way, show that  $d_M \leq d_Z$ .

One can show the second part of the Lemma in the same way, by considering a minimum weight  $X$ -logical,  $v$ , and the corresponding  $\bar{v} \in \ker(H_Z^\top) \setminus \text{rs}(M_Z)$ , which has the same weight.  $\square$

Certain different polynomials produce codes with equivalent parameters. Observing these equivalences can speed up code searches. We first observe that, trivially, if we permute  $A$ ,  $B$  and  $C$ , we obtain an equivalent code. Furthermore, taking the transpose of  $A$ ,  $B$  and  $C$  also results in an equivalent code: the ranks of  $H_X$  and  $H_Z$  can easily be shown to be unchanged, and the distances  $d_X$ ,  $d_Z$ , and  $d_M$  are unchanged as a result of Lemma 2. We finally show that, if one of the polynomials has a common

monomial factor, this can be removed without affecting the code parameters. Without loss of generality, we treat  $A$  as the polynomial that can be simplified in this way.

**Lemma 3.** *Consider the  $[[n, k, d]]$  TT code defined by polynomials  $A$ ,  $B$  and  $C$ , with parity check matrices  $H_X$  and  $H_Z$ . Suppose that  $A = \alpha^\top \tilde{A}$  for some monomial  $\alpha$  and polynomial  $\tilde{A}$ . Then define the TT code with parity check matrices  $\tilde{H}_X$  and  $\tilde{H}_Z$ , based on polynomials  $\tilde{A}$ ,  $B$  and  $C$ . This defines an  $[[n, k, d]]$  code. Additionally, the distances  $d_X$  and  $d_Z = d_M$  are separately preserved.*

*Proof.* The fact that  $n$  is unchanged is trivial. We show that  $k$  is unchanged. Notice that:

$$\tilde{H}_X = [\alpha A | B | C] = [A | B | C] \begin{bmatrix} \alpha & 0 & 0 \\ 0 & 1 & 0 \\ 0 & 0 & 1 \end{bmatrix}, \quad (26)$$

and so, owing to the fact that  $\alpha$  is invertible,  $\tilde{H}_X$  is related to  $H_X$  by an invertible matrix, meaning that  $\text{rk} \tilde{H}_X = \text{rk} H_X$ . Now consider some vector  $v \in \ker H_Z$ . It can be easily seen that:

$$\begin{bmatrix} 1 & 0 & 0 \\ 0 & \alpha & 0 \\ 0 & 0 & \alpha \end{bmatrix} v \in \ker \tilde{H}_Z. \quad (27)$$

Hence, once again owing to the invertibility of  $\alpha$ , we have an isomorphism between  $\ker H_Z$  and  $\ker \tilde{H}_Z$ . Therefore,  $\text{rk} H_Z = \text{rk} \tilde{H}_Z$ . Hence,  $k = n - \text{ker} H_X - \text{ker} H_Z = n - \text{ker} \tilde{H}_X - \text{ker} \tilde{H}_Z$  is unchanged.

Now consider the distances  $d_X$  and  $d_Z$ . Suppose that  $v_Z = [v_1^\top, v_2^\top, v_3^\top]^\top \in \ker H_X$  is a minimum-weight logical operator. Then clearly  $v'_Z = [v_1^\top \alpha, v_2^\top, v_3^\top]^\top \in \ker \tilde{H}_X$ . Hence,  $v'_Z$  represents either a logical or a  $Z$ -stabilizer of the code  $(\tilde{H}_X, \tilde{H}_Z)$ . If it is a stabilizer then it is in the image of  $\tilde{H}_Z^\top$ , i.e.,  $v'_Z = \tilde{H}_Z^\top w$ , for some  $w = [w_1^\top, w_2^\top, w_3^\top]^\top$ . But  $v'_Z = \text{diag}[\alpha^\top, 1, 1]v_Z$ . Hence:

$$v_Z = \begin{bmatrix} \alpha & 0 & 0 \\ 0 & 1 & 0 \\ 0 & 0 & 1 \end{bmatrix} \tilde{H}_Z^\top \begin{bmatrix} 1 & 0 & 0 \\ 0 & \alpha^\top & 0 \\ 0 & 0 & \alpha^\top \end{bmatrix} \left( \begin{bmatrix} 1 & 0 & 0 \\ 0 & \alpha & 0 \\ 0 & 0 & \alpha \end{bmatrix} \begin{bmatrix} w_1 \\ w_2 \\ w_3 \end{bmatrix} \right) \quad (28)$$

$$= H_Z^\top w' \quad (29)$$

where  $w' = [w_1^\top, w_2^\top \alpha^\top, w_3^\top \alpha^\top]^\top$ . Hence,  $v_Z \in \text{im}H_Z^\top$ , contradicting the assumption that it is a logical operator of the code  $(H_X, H_Z)$ . Hence, we conclude that  $v'_Z$  is a logical operator of  $(\tilde{H}_X, \tilde{H}_Z)$ . Therefore:

$$\tilde{d}_Z \leq |v'_Z| = |\alpha v_1| + |v_2| + |v_3| = |v_Z| = d_Z, \quad (30)$$

where  $\tilde{d}_Z$  and  $d_Z$  are  $Z$ -distances of the modified and original codes, respectively. We can similarly show that  $d_Z \leq \tilde{d}_Z$ , and so the  $Z$ -distances are equivalent. By Lemma 2, we find that  $\tilde{d}_M = d_M$  as well. An analogous argument shows that  $\tilde{d}_X = d_X$ . Hence all distances are equivalent.  $\square$

We finish this section by listing some TT codes, based on weight-3 polynomials (i.e., those with three distinct terms), that display parameters that outperform those of common topological codes in 2D and 3D, such as the surface code and 3D toric code. In Table I, we list some examples of TT codes found through a random numerical search, along with their parameters and the matrices  $A$ ,  $B$  and  $C$  that define each code. We list both the  $X$  and  $Z$  distances, which are upper bounds based on numerical searches performed using the BP+OSD decoder in the technique outlined in Section 6 of Ref. [12], and a custom version of QDR [45] using software from the CSSLO repository [46]. We list further TT code examples in Appendix A.

## B. 3D Layout of TT codes

A conceptual aid exists for bivariate bicycle codes upon laying them out on a 2D grid, with additional long-range connections and with periodic boundary conditions. Similarly, we can locally lay out the Tanner graphs of the TT codes on a 3D cubic lattice with long-range connections. This is most readily illustrated using the 3DTC, which is a special case of a TT code with  $A = 1+x$ ,  $B = 1+y$  and  $C = 1+z$ . We lay the code out on a lattice with qubits on the edges,  $X$ -checks on the vertices and  $Z$ -checks on the faces. This structure is shown in Fig. 1. We also can assign meta-checks to the 3-cells (cubes) of the lattice (see Fig. 6 of Section V C).

Also similar to the case of bivariate bicycle codes, the 3D layout elucidates a useful monomial labelling. For a general TT code, we define three blocks of data qubits, labelled L, C and R which correspond to the Left, Center and Right blocks of columns in  $H_X$  and  $H_Z$ . In Fig. 1, the L, C and R qubits inhabit edges pointing in the  $x$ ,  $y$  and  $z$  directions, respectively (they are coloured grey, black and white). The number of data qubits in each block is given by  $\ell_{\text{mp}}$ , and as such, we can label each qubit in one of the blocks by a distinct monomial  $\alpha \in \mathcal{M} \equiv \{x^i y^j z^k : i = 1, \dots, \ell, j = 1, \dots, m, k = 1, \dots, p\}$ .

There are also  $\ell_{\text{mp}}$   $X$ -checks (rows of  $H_X$ ), and we also label each of these with a monomial in  $\mathcal{M}$ . We do so in such a way that  $X$ -check  $\alpha \in \mathcal{M}$  is connected to

L qubits  $A_i \alpha$  (for all terms  $A_i$  in  $A$ ), C qubits  $B_i \alpha$ , and R qubits  $C_i \alpha$ . For the 3DTC, this is shown in Fig. 1(a). We explicitly consider an  $X$ -check labelled by  $xz \in \mathcal{M}$ . Meanwhile, we have three sets of  $Z$  checks, which correspond to the three blocks of rows from  $H_Z$ . We will refer to these checks, and colour them in Fig. 1(b), as  $Z_a$  (red),  $Z_b$  (blue), and  $Z_c$  (yellow) checks. Geometrically, in the 3DTC, these checks correspond to square faces oriented in three orthogonal directions. The checks in each of these three sets are labelled with monomials from  $\mathcal{M}$ . The  $Z_a$ ,  $Z_b$  and  $Z_c$  checks are connected to CR, LR and LC qubits, respectively via terms from  $A^\top$ ,  $B^\top$  or  $C^\top$ . In Fig. 1(b) we consider explicit examples for checks from each set. There are, finally,  $\ell_{\text{mp}}$  meta-checks resulting from rows in  $M_Z$ , which we once again label by monomials from  $\mathcal{M}$ . Meta-check  $\alpha$  is such that it is “connected to”  $Z_a$ -checks  $A^\top \alpha$ ,  $Z_b$ -checks  $B^\top \alpha$ , and  $Z_c$  checks  $C^\top \alpha$  (see Fig. 6). By this we mean that the product of all the  $Z$  checks connected to  $\alpha$  is the identity.

A TT code with weight-3 polynomials has 3 additional long-range connections for each  $X$ -check relative to the 3DTC, and 2 extra long-range connections for each  $Z$ -check. However, the code’s Tanner graph may still possess a 3D toric layout: it does so whenever it possesses a spanning subgraph isomorphic to the Cayley graph of  $\mathbb{Z}_\mu \times \mathbb{Z}_\lambda \times \mathbb{Z}_\nu$  for integers  $\mu, \lambda, \nu$ . Its Tanner graph may also be composed of a single or multiple connected components, though in this paper we focus on those with only a single connected component. In Appendix A we report conditions for codes to possess a 3D toric layout and a connected Tanner graph.

## III. SINGLE-SHOT DECODING OF TT CODES UNDER PHENOMENOLOGICAL NOISE

We wish to investigate TT code performance numerically, and we begin by performing simulations under a simplified, “phenomenological” noise model. We separately perform  $Z$  and  $X$  memory experiment simulations: we prepare all logical qubits in the  $|0\rangle$  state (resp. the  $|+\rangle$  state), perform stabilizer measurement for  $r$  rounds, then measure out all data qubits in the  $Z$  basis (resp.  $X$  basis) to determine the state of the logical qubits at the end of the experiment. In between rounds, single-qubit depolarising noise channels are applied to data qubits with strength  $p$  and, independently, each measurement suffers a classical readout error with probability  $p$ . Our simulations were carried out using the Python packages LDPC [47] and Stim [48].

In Fig. 2(a), we present data for the  $X$  memory experiments, examining the codes presented in Table I. We plot logical error probability (per round) for each code, without normalising for the number of logical qubits. We choose to run the memory experiment simulations for  $r = 2d$  rounds, where  $d$  is the code distance. Decoding is performed using a BP+OSD decoder (without any windowing) [47, 49] and we perform quadratic fits to the

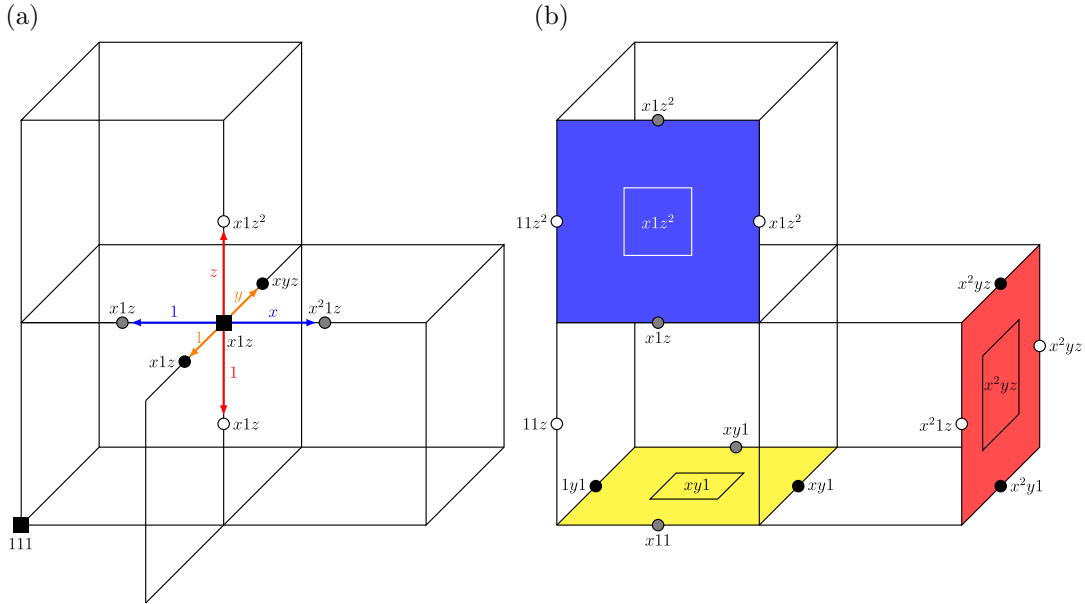


FIG. 1. Layout of the 3D toric code on a cubic lattice. The code’s defining polynomials are  $A = 1 + x$ ,  $B = 1 + y$ ,  $C = 1 + z$ . Qubits are placed on edges,  $X$ -checks on vertices and  $Z$ -checks on faces. (a)  $X$ -checks are connected to adjacent data qubits by terms in  $A$  (for Left qubits, shaded grey),  $B$  (for Centre qubits, shaded black), or  $C$  (for Right qubits, shaded white). Example  $X$ -check  $x1z$  and its connected qubits is shown. (b)  $Z$ -checks fall into three families, coloured red ( $Z_a$ ), blue ( $Z_b$ ), and yellow ( $Z_c$ ), respectively. Each family corresponds to an orthogonal orientation of a plane in the lattice.  $Z$ -checks are connected to data qubits on the edges surrounding the face by terms from (transposes of) two of the three polynomials. As an example, the red  $Z$ -checks are connected to Centre qubits by terms in  $C^\top$  and Right qubits by terms in  $B^\top$ . Three example  $Z$ -checks and their connected qubits are shown. TT codes can be locally laid out on the same 3D cubic lattice, with additional long-range connections. For TT codes built from weight-3 polynomials, the  $X$  checks gain 3 long-range connections, and the  $Z$  checks gain 2 long-range connections.

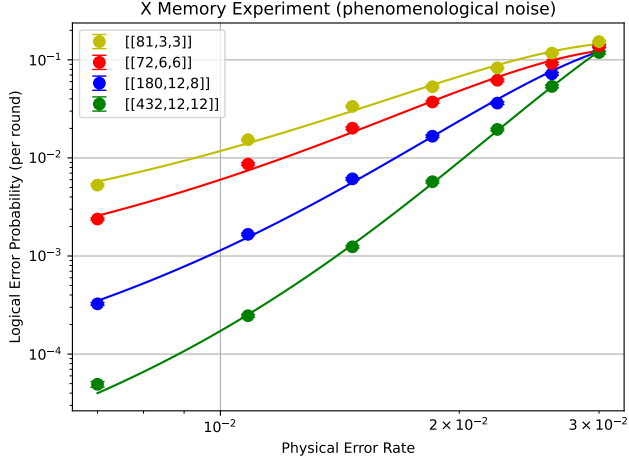
data. We additionally plot the results for the  $[[81, 3, 3]]$  3DTC for comparison, showing that all TT codes tested out-perform this code for the range of physical error rates examined.

We perform an estimate of the threshold for the  $X$  memory experiment – the crossing-point of the three TT code curves in Fig. 2(a) – which is at around 3.0%. We also determine pseudo-thresholds for the three codes – the solution to the break-even equation  $p_L(p) = p$ , where  $p$  is the physical error rate and  $p_L$  is the per-round logical error rate in the  $X$  memory experiment. (Note we define the pseudo-threshold differently here to in Section IV, where we define it as the solution to  $p_L(p) = kp$ . Under phenomenological noise, the solutions to this latter equation are far above threshold and hence have little meaning.) We find the following estimates for the pseudo-thresholds under this particular error channel.  $[[81, 3, 3]]$  3D toric code: 0.87%;  $[[72, 6, 6]]$  TT code: 1.3%;  $[[180, 12, 8]]$  TT code: 1.9%;  $[[432, 12, 12]]$  TT code: 2.3%.

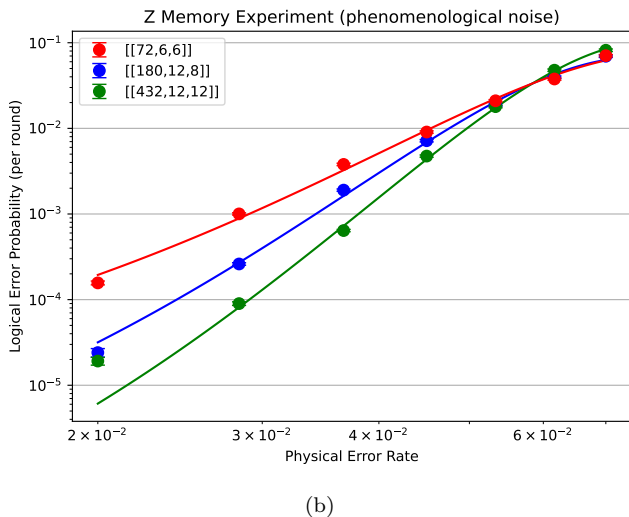
We then test for single-shot decodability in the  $Z$  memory experiment. We test for single-shot properties using an overlapping window method and a BP+OSD decoder [25, 26, 50, 51] (see the LDPC Python package for an implementation [47, 49]). The idea of an overlapping window method is that we perform decoding inside

a “window” of  $w$  measurement rounds. The subset of the syndrome that was extracted in the rounds that fall within this window is passed to a BP+OSD decoder and a most-likely correction of that restricted syndrome is determined. We then consider a “commit region” of the first  $c$  rounds in the window. Any component of the correction in the window that lies in the commit region is committed to, while the component outside of this region is discarded. The window is then slid  $c$  rounds into the future and decoding performed again, in the same way. We refer to this as a  $(w, c)$  windowing strategy. Since we are decoding with restricted information (ignoring the check measurements outside of each window), this strategy does not in general perform as well as decoding with full syndrome information. However, the latter’s temporal overhead scales with the number of rounds, which becomes impractical. Single-shot codes, meanwhile, allow for a threshold to be maintained even as the window size is kept constant and the total number of syndrome extraction rounds is increased, which leads to much lower decoding overheads [52].

In Fig. 2(b), we present data for the  $Z$  memory experiment simulations, examining codes from Table I, and employing a  $(2, 1)$  windowing strategy. Under this strategy, we observe a threshold for  $Z$  memory of 5.8%. The pseudo-thresholds of the three codes (for  $Z$  memory) sit



(a)



(b)

FIG. 2. Performance of the TT codes under a phenomenological noise model. We present logical error rates (LERs) in memory experiments performed over  $2d_Z$  rounds of syndrome measurements. (a) TT and 3DTC performance in  $X$  memory experiments, for small instances of TT codes from Table I. For all instances considered, the TT codes perform better, while encoding more logical qubits than the  $[[81, 3, 3]]$  3DTC (yellow). Decoding was performed with BP+OSD-CS0 over the full syndrome history. (b) TT code LERs in  $Z$  memory experiments with a  $(2,1)$  windowing strategy. The asymmetric distances of the TT codes lead to strong error suppression in the  $X$  error channel ( $Z$  memory), resulting in order of magnitude reductions in the LER, compared to the  $Z$  error channel ( $X$  memory).

above this threshold and are:  $[[72, 6, 6]]$  TT code: 7.0%;  $[[180, 12, 8]]$  TT code: 6.8%;  $[[432, 12, 12]]$  TT code: 6.6%. We note that in the low noise regime the decoder struggled to continue suppressing errors. For all error rates,  $Z$  memory simulations were significantly slower than  $X$  memory simulations.

We also examine the  $Z$  memory performance under

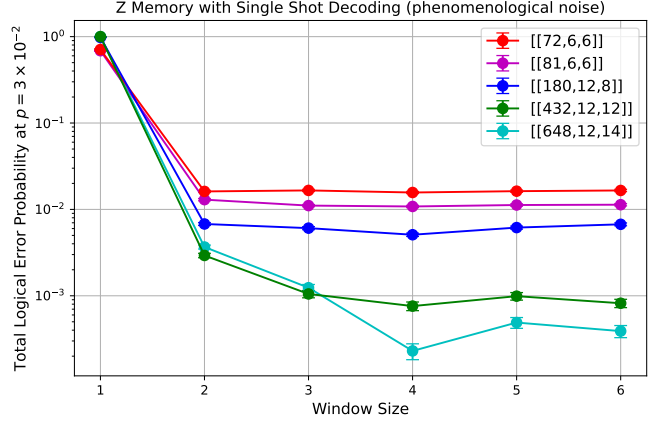


FIG. 3. Total logical error probability for  $Z$  memory vs window size used in the overlapping window strategy, for several TT codes, listed in Table V. The plateaus demonstrates that optimal decoding performance can be obtained with a fixed window and commit size, indicating full syndrome histories do not need to be considered. Simulations were performed under a phenomenological noise model with physical noise rate  $p = 3 \times 10^{-2}$  and  $N = 14$  rounds. The decoding windows had commit regions of size 1.

different windowing strategies. In Fig. 3 we present results for a  $(w, 1)$  windowing strategy, where we vary  $w$  between 1 and 6. We present results for a range of codes from Table I and Table V. We fix the total number of syndrome extraction rounds to be  $r = 14$  and the physical error rate to be  $p = 3 \times 10^{-2}$ . We find that the logical error rates for  $Z$  memory experiments for the TT codes rapidly plateau as we increase the window size, meaning that the performance of the decoder does not continue to increase as more syndrome information is taken into account during each round of decoding, indicating single-shot properties.

#### IV. CIRCUIT LEVEL NOISE SIMULATIONS

We conduct  $X$  and  $Z$  memory simulations, and verify the existence of  $(w, c)$  single-shot decodability under a circuit level noise model for both the TT and 3D Toric codes. We utilise depth-13, interleaved syndrome measurement circuits detailed in Appendix B. We define three sets of  $n/3$   $Z$ -measure qubits (for measuring  $Z_a$ ,  $Z_b$  and  $Z_c$  checks), and for two of these, we alternate using them for  $Z_b$  and  $Z_c$  checks in adjacent rounds, again to minimise circuit-depth, lastly we use  $n/3$   $X$ -measure qubits. However, we note that omitting resets on the  $X$ -measure qubits to minimise the circuit depth, likely has a minimal effect on memory performance [53, 54]. Overall we use  $4n/3$  measure qubits (for  $n$  data qubits in the code). In Appendix B, we prove that the circuits result in the required transformations of the stabilizer tableaux. We stress that we have not optimised the ordering of these circuits for circuit-level distance, and fur-

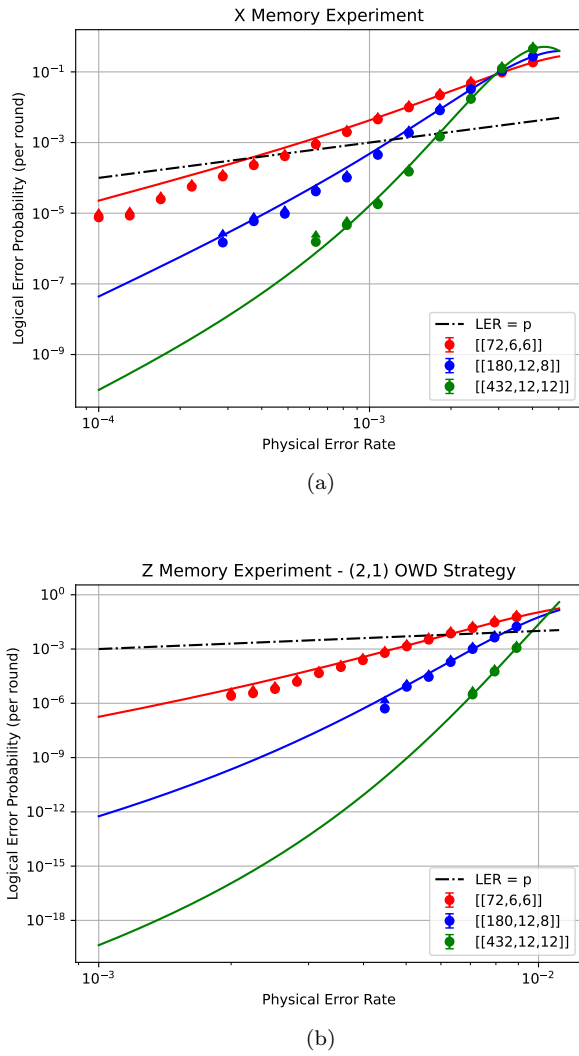


FIG. 4. Performance of the TT codes under circuit level noise. (a) Logical error rate per round in  $X$  memory experiments, decoded using BP+OSD-CS30, over the full syndrome history. A crossing between instances of TT codes is found at a physical error rate of  $2.9 \times 10^{-3}$ . (b) Logical error rate per round in  $Z$  memory experiments. Decoding was performed using a  $(2,1)$  overlapping window strategy (Sec. III) with BP+OSD-CS0. We find a crossing at  $1.1 \times 10^{-2}$ . Arrowheads show the upper limit of the logical error rate.

ther improvements could potentially be made.

We use a standard depolarizing, circuit-level noise model, where all errors occur with probability  $p$ . All qubits undergo bit/phase flip errors after resets, and depolarising noise while idling. All qubits also undergo two-qubit (correlated) depolarising errors after each CNOT gate. Lastly, measure qubits undergo measurement flips (implemented via  $X$  or  $Z$  errors on measure qubits prior to measurement). The results are shown in Table II. For toric code simulations, we use a modified version of the syndrome measurement circuit, omitting gates associated with  $J_3$  terms, where  $J \in \{A, B, C\}$ , in the polynomials

Eqns.(8-10). These circuits may not be optimal for the 3DTC, but we omit noise channels on the idling layers thereby introduced. Hence, our 3DTC results are likely an upper-bound on the code performance.

For memory experiments, we perform  $r$  rounds of syndrome measurement, and compute the logical error rate per round ( $p_L$ ) with the formula:

$$p_L = 1 - (1 - P_L)^{\frac{1}{r}} \quad (31)$$

where  $P_L$  is the total number of logical errors over all shots. To extrapolate the code performance to lower error rates, we fit trend lines using the *ansatz*,  $p_L = p_{circ}^{d_{circ}/2} e^{c_0 + c_1 p + c_2 p^2}$  [12], and numerically compute the coefficients using SciPy [55]. The parameter  $d_{circ}$  is the upper-bound on the circuit level distance, obtained by finding the minimum weight error that triggers no detectors in the detector matrix [56]. The detector matrix is obtained using stimbposd [57] and the minimum weight error was found using the technique in Section 6 of Ref. [12] and BP+OSD [47]. For large detector matrices, for example in the  $[[432, 12, 12]]$  code, BP+OSD struggles to find low weight errors when estimating circuit-level distance. In that case, in fits we use an effective circuit distance  $d'_{circ} \leq d_{circ}$ , the maximum value that produces a trend line that fits the data points. Due to the asymmetry in the  $X$  and  $Z$  distances, the *limiting* distance is the  $Z$  distance. As such, in Table II we present crossing points for the  $X$  memory experiments, which serve as an estimate for a threshold for the TT codes. In the following, we do not normalise for the number of logical qubits encoded, hence the error rates include correlated errors within a code patch.

### A. Simulation Results

In  $X$  memory experiments over  $d_Z + 1$  rounds, using BP+OSD-CS30 with a parallel BP schedule, we observe a crossing between various small instances of TT codes at  $2.9 \times 10^{-3}$ . This is slightly higher than the crossing for the Toric code, which occurs at  $2.7 \times 10^{-3}$ . We also compute the pseudo-thresholds, the physical error rate below which the code suppresses more errors than an equivalent number of un-encoded qubits. This is the solution of the break-even equation  $p_L(p) = kp$  [12], with  $k$  the number of logical qubits, and  $p$  the physical error rate. We find that the pseudo-thresholds of TT codes are consistently higher than those of 3DTCs. Our simulations suggest that the  $[[432, 12, 12]]$  TT code has a logical error rate  $\leq 10^{-9}$  at a physical error rate of  $10^{-4}$ ; meaning, it can preserve 12 logical qubits for over 100 million syndrome cycles, in the low noise regime. We also note that the effective distances  $d'_{circ}$ , used to compute the trend lines are slightly lower than the computed circuit distances.

For  $Z$  memory experiments, which are limited by  $d_X$ , we evaluate the logical error rates over 13 rounds of syndrome measurement, with BP+OSD-CS0 and a paral-

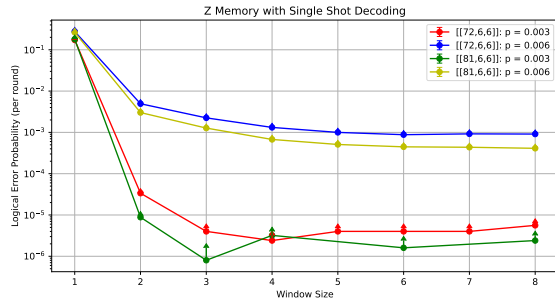


FIG. 5. Logical error plateaus, for a commit size of 1 and varying window size, under a circuit level noise model for small TT codes. The  $[[72, 6, 6]]$  and  $[[81, 6, 6]]$  codes both exhibit single-shot decodability in the  $X$  error channel, at error rates of  $p = 0.003$  and  $p = 0.006$ . At  $p = 0.003$ , the plateau begins around  $w = 3$ , however at  $p = 0.006$  the plateau begins around  $w = 5$ .

lel BP schedule. Note that  $Z$ -memory decoding is more complex, with higher-weight syndromes and BP failing more frequently. For this reason, we reduce the order of the OSD post-processing step to reduce runtime. For these simulations, we use a  $(2, 1)$  overlapping widow decoder to verify the existence of a crossing, while employing single-shot decoding. Under these circumstances we find a crossing at a physical error rate of  $1.06 \times 10^{-2}$ , and pseudo-thresholds at approximately 1%. The error suppression in the  $X$  error channel is thus far greater than in the  $Z$  channel, even using windowing and a lower OSD order. Note that we find that  $d'_{circ}$  is significantly lower than the computed circuit distances. Possible reasons for this are discussed subsequently.

We perform  $Z$  memory, single-shot experiments under a  $(w, 1)$  strategy for various values of  $w$  and show that a logical error plateau is recovered even under a circuit level noise model. This suggests that TT codes retain single-shot capabilities in realistic settings. In Fig.5 we explore sub-threshold noise regimes while varying the window size. We observe that the code performance rapidly plateaus as we increase the window size, albeit at a slower rate for larger  $p$ . That is, at a physical error rate of  $p = 6 \times 10^{-3}$  the LER plateau occurs at around  $w = 5$ , whereas at a physical error rate of  $p = 3 \times 10^{-3}$  the LER plateau begins at around  $w = 3$ . It is also interesting to note that the  $[[72, 6, 6]]$  code has a higher logical error rate than the  $[[81, 6, 6]]$  despite having the same  $X$ -distance and fewer qubits. We suspect this discrepancy is caused by structural differences in the Tanner graphs of the two codes. Of relevance could be the fact that the  $[[81, 6, 6]]$  code has a toric layout, while the  $[[72, 6, 6]]$  code does not. A thorough analysis is deferred to future work.

We note that the presence of short cycles between  $Z$ -checks in the Tanner graph likely degrade the performance of the decoder in these experiments. The BP algorithm assumes a tree-like Tanner graph [58], in which

there are no cycles. However, quantum codes expressly violate this condition [59]. The  $Z$ -checks in TT codes are high weight and have greater overlapping support, thereby increasing the number of short-cycles. This leads to BP failing frequently, and falling back to OSD to find a correction, degrading performance and increasing runtime. This can be mitigated in two ways, firstly, using automorphism based decoders such as aut-dec [60] which can reduce the impact of short-cycles in BP with low overhead. Alternatively, one can eschew BP entirely and use decoders such as Tesseract [61] which use graph search techniques where performance is not degraded by short cycles. However, exploration of alternative decoders is deferred to future work.

## V. LOGIC GATES IN TRIVARIATE TRICYCLE CODES

In this Section, we explore logic gates that can be applied within TT codes via automorphisms or transversal/constant-depth circuits of  $CZ/CCZ$  gates. We begin by noting the structure of the logical qubits in TT codes (this applies to other 3-block codes as well). We will find that the logical qubits can fall into one of three sets, with logical Pauli operators for each set mutually commuting between the three sets.

Let  $X(P, Q, S)$ , for polynomials  $P, Q$  and  $S$ , represent an  $X$  operator with support on qubits in the L block corresponding to all monomial terms in  $P$ , and similarly for  $Q$  in the C block and  $S$  in the R block (recall that qubits in each block can be labelled by monomials in  $\mathcal{M}$ ). We similarly define  $Z(\bar{P}, \bar{Q}, \bar{S})$  as a  $Z$  operator with support on  $\bar{P}$  qubits in the L block,  $\bar{Q}$  qubits in the C block, and  $\bar{S}$  qubits in the R block. We have the following:

**Lemma 4.**  $X(P, Q, S)$  and  $Z(\bar{P}, \bar{Q}, \bar{S})$  anti-commute if and only if  $1 \in PP^\top + Q\bar{Q}^\top + S\bar{S}^\top$ .

The proof is analogous with a similar one in Ref. [12], and we provide it in Appendix A for completeness.

Now suppose we can find polynomials  $f, g, h$  and  $j$  that obey:

$$Af = Bf = Cf = 0 \quad (32)$$

$$Ch + Bj = Cg + Aj = Bg + Ah = 0. \quad (33)$$

Note that this implies that  $f \in \ker A \cap \ker B \cap \ker C$  and  $[g^\top, h^\top, j^\top]^\top \in \ker[0 \ C \ B] \cap \ker[C \ 0 \ A] \cap \ker[B \ A \ 0]$ . According to Lemma 1, these sets cannot both be trivial (since  $k > 0$ ).

Then the following are all logical operators, where  $\alpha \in \mathcal{M}$ :

$$\begin{aligned} \bar{X}_\alpha^{(1)} &= X(\alpha f, 0, 0), \quad \bar{Z}_\alpha^{(1)} = Z(\alpha h^\top, \alpha g^\top, 0), \\ \bar{X}_\alpha^{(2)} &= X(\alpha g, \alpha h, \alpha j), \quad \bar{Z}_\alpha^{(2)} = Z(0, \alpha f^\top, 0), \\ \bar{X}_\alpha^{(3)} &= X(0, 0, \alpha f), \quad \bar{Z}_\alpha^{(3)} = Z(0, \alpha j^\top, \alpha h^\top). \end{aligned} \quad (34)$$

Code Family	Threshold	$[[n, k, d]]$	Circuit Distance	Pseudo-threshold ( $\times 10^{-3}$ )
3D Toric	$2.7 \times 10^{-3}$	$[[81, 3, 3]]$	$\leq 3$	0.8
		$[[375, 3, 5]]$	$\leq 5$	1.8
		$[[1029, 3, 7]]$	$\leq 7$	2.0
Trivariate Tricycle	$2.9 \times 10^{-3}$	$[[72, 6, 6]]$	$\leq 4$	1.2
		$[[180, 12, 8]]$	$\leq 7$	2.3
		$[[432, 12, 12]]$	$\leq 12$	2.5

TABLE II. Threshold, circuit distance and pseudo-thresholds for 3D Toric and TT codes, in  $X$  memory experiments (the basis which limits code performance). The results show that the two codes are very close in terms of performance. The circuit distances are those computed by the method discussed in Sec.IV.

We note that these logical Pauli operators belong to one of three sets, which we label with superscripts (and which are akin to the primed and unprimed blocks in Ref. [12]). To see that these are logical operators, note that  $X(P, Q, S)$  commutes with all  $Z$  stabilizers whenever  $CQ + BS = CP + AS = BP + AQ = 0$  (due to Lemma 4). Hence  $X_{\alpha}^{(1)}$  and  $X_{\alpha}^{(3)}$  clearly commute with all  $Z$  stabilizers, because of Eqn. 32, while  $X_{\alpha}^{(2)}$  does so, from Eqn. 33.  $Z(P^{\top}, Q^{\top}, S^{\top})$  commutes with all  $X$  stabilizers whenever  $AP + BQ + CS = 0$ . Hence, it can be seen that  $Z_{\alpha}^{(i)}$  commutes with all  $X$  stabilizers, for  $i = 1, 2, 3$ .

It can be seen that all  $\bar{X}_{\alpha}^{(i)}$  commute with all  $\bar{Z}_{\beta}^{(j \neq i)}$ . For example,  $\bar{X}_{\alpha}^{(2)}$  and  $\bar{Z}_{\beta}^{(1)}$  commute because  $\alpha\beta^{\top}gh + \alpha\beta^{\top}hg + \alpha j 0^{\top} = 0$ . Note that the particular choice of logical groupings into the three sets is not unique. And indeed, the logical operators  $\bar{X}_{\alpha}^{(i)}$  and  $\bar{Z}_{\beta}^{(j)}$  will only be able to anti-commute if  $fh \neq 0$ . This is because  $\bar{X}_{\alpha}^{(i)}$  and  $\bar{Z}_{\beta}^{(i)}$  form an anti-commuting pair whenever  $\alpha\beta^{\top} \in fh$ . If  $fh = 0$ , we will not be able to find any conjugate logical operators within the sets chosen above. In such cases, we can find two more choices for the logical sets: one which assumes  $fg \neq 0$  and another which assumes  $fj \neq 0$ . If  $fg \neq 0$ , we have:

$$\begin{aligned} \tilde{X}_{\alpha}^{(1)} &= X(0, \alpha f, 0), \quad \tilde{Z}_{\alpha}^{(1)} = Z(\alpha h^{\top}, \alpha g^{\top}, 0), \\ \tilde{X}_{\alpha}^{(2)} &= X(\alpha g, \alpha h, \alpha j), \quad \tilde{Z}_{\alpha}^{(2)} = Z(\alpha f^{\top}, 0, 0), \\ \tilde{X}_{\alpha}^{(3)} &= X(0, 0, \alpha f), \quad \tilde{Z}_{\alpha}^{(3)} = Z(\alpha j^{\top}, 0, \alpha g^{\top}), \end{aligned} \quad (35)$$

while if  $fj \neq 0$  we have:

$$\begin{aligned} \hat{X}_{\alpha}^{(1)} &= X(\alpha f, 0, 0), \quad \hat{Z}_{\alpha}^{(1)} = Z(\alpha j^{\top}, 0, \alpha g^{\top}), \\ \hat{X}_{\alpha}^{(2)} &= X(\alpha g, \alpha h, \alpha j), \quad \hat{Z}_{\alpha}^{(2)} = Z(0, 0, \alpha f^{\top}), \\ \hat{X}_{\alpha}^{(3)} &= X(0, \alpha f, 0), \quad \hat{Z}_{\alpha}^{(3)} = Z(0, \alpha j^{\top}, \alpha h^{\top}). \end{aligned} \quad (36)$$

Not all codes we find admit a complete decomposition into one of the choices of logical sets given above.

All codes we investigate have some choice of  $f$  and  $[g^{\top}, h^{\top}, j^{\top}]^{\top}$  that obey Equations 32 and 33 respectively, but it may be the case that none of the corresponding logical sets (Equations 34, 35 or 36) cover all logical qubits in the code. In Table V of Appendix A, we report whether each code found admits a decomposition of a full set of  $k$  logicals into one of the logical sets above (Equations 34, 35 or 36).

### A. Shift Automorphisms

Owing to the translational invariance of the TT codes, any shift automorphism that maps L, C, and R qubits  $\alpha \mapsto \beta\alpha$  is a valid logical operation. This is a “shift” automorphism because it shifts the entire lattice (Fig. 1), mapping each qubit  $\alpha$  in each block to a new location,  $\beta\alpha$ . Consider an  $X$ -check corresponding to monomial  $\alpha \in \mathcal{M}$ . This can be written as  $X(A\alpha, B\alpha, C\alpha)$ , since it acts non-trivially on those data qubits in the L block connected to it by terms in  $A$ , and similarly for data qubits in the C and R blocks, with polynomials  $B$  and  $C$ , respectively. The shift automorphism transforms this  $X$  stabilizer generator as:

$$X(A\alpha, B\alpha, C\alpha) \mapsto X(A\beta\alpha, B\beta\alpha, C\beta\alpha). \quad (37)$$

Similarly, observing the rows of  $H_Z$ , we may see how  $Z_a$ -,  $Z_b$ -, and  $Z_c$ -stabilizer generators are written. These are transformed by the shift automorphism as:

$$\begin{aligned} Z_a(0, C^{\top}\alpha, B^{\top}\alpha) &\mapsto Z_a(0, C^{\top}\beta\alpha, B^{\top}\beta\alpha), \\ Z_b(C^{\top}\alpha, 0, A^{\top}\alpha) &\mapsto Z_b(C^{\top}\beta\alpha, 0, A^{\top}\beta\alpha), \\ Z_c(B^{\top}\alpha, A^{\top}\alpha, 0) &\mapsto Z_c(B^{\top}\beta\alpha, A^{\top}\beta\alpha, 0). \end{aligned} \quad (38)$$

Notice that the automorphism simply permutes checks within a class ( $X$ ,  $Z_a$ ,  $Z_b$  or  $Z_c$ ), and hence preserves the code space.

If we can find a decomposition of the logical operators into one of the three logical sets introduced above (Equations 34, 35 or 36), then the shift automorphisms can be

understood as transforming between the logical operators within a set. For example, the  $\alpha \mapsto \beta\alpha$  automorphism maps  $\bar{X}_\alpha^{(i)} \mapsto \bar{X}_{\beta\alpha}^{(i)}$  and  $\bar{Z}_\alpha^{(i)} \mapsto \bar{Z}_{\beta\alpha}^{(i)}$  for  $i = 1, 2, 3$ . However, these automorphisms cannot map between operators in different sets.

To implement such shift automorphisms via a low-depth circuit, we perform SWAP gates between data qubits and  $Z$ -measure qubits in the following pattern:

$$q(L, \alpha) \leftrightarrow q_Z(a, \beta_1\alpha) \leftrightarrow q(L, \beta_2\beta_1\alpha) \quad (39)$$

$$q(C, \alpha) \leftrightarrow q_Z(b, \beta_1\alpha) \leftrightarrow q(C, \beta_2\beta_1\alpha) \quad (40)$$

$$q(R, \alpha) \leftrightarrow q_Z(c, \beta_1\alpha) \leftrightarrow q(R, \beta_2\beta_1\alpha), \quad (41)$$

where we label data qubits  $q(B, \alpha)$  for block label B and monomial label  $\alpha$ , and we label  $Z$ -measure qubits  $q_Z(b, \alpha)$ , where  $b$  is the  $Z$ -measure block label. This series of SWAP gates permutes  $Z$ -measure qubits within each block ( $a, b$  and  $c$ ) and performs a shift of the data qubits  $\alpha \mapsto \beta_2\beta_1\alpha$  within each of the data qubit blocks (L, C and R).

If we wish to avoid adding additional connections between qubits, we must alter this pattern of SWAP gates slightly. Firstly, note that, from the necessary structure of the syndrome measurement circuits, we can apply gates between  $q(L, \alpha)$  and  $q_X(A_i^\top \alpha)$  (for any  $i$ ) and similarly between  $q(C, \alpha)$  and  $q_X(B_i^\top \alpha)$  and  $q(R, \alpha)$  and  $q_X(C_i^\top \alpha)$ , where we once again label  $X$ -measure qubits with only a monomial label. We may also perform gates between  $q(L, \alpha)$  and  $q_Z(b, C_i\alpha)$  or  $q_Z(c, B_i\alpha)$  and so on. Suppose we wish to perform a shift automorphism of the data qubits given by  $\alpha \mapsto A_j A_i^\top \alpha$  (for all data qubit blocks). We can perform the following depth-2 circuit of SWAP gates using existing connections to implement this:

$$q(L, \alpha) \leftrightarrow q_X(A_i^\top \alpha) \leftrightarrow q(L, A_j A_i^\top \alpha) \quad (42)$$

$$q(C, \alpha) \leftrightarrow q_Z(c, A_j\alpha) \leftrightarrow q(C, A_i^\top A_j\alpha) \quad (43)$$

$$q(R, \alpha) \leftrightarrow q_Z(b, A_j\alpha) \leftrightarrow q(R, A_i^\top A_j\alpha). \quad (44)$$

One can easily find a similar, depth-2 pattern of SWAP gates for shifts by  $B_j B_i^\top$  and  $C_j C_i^\top$ . If we assume the Tanner graph is connected, these shift automorphisms generate the entire group of shifts  $\alpha \mapsto \beta$ .

## B. Logical CZ gates between code blocks

We now focus on logical gates that can be implemented between identical code blocks. Recent qLDPC codes have been found that allow for certain Clifford gates to be performed within or between code blocks [32]. For BB codes, Ref. [35] explains methods for verifying that a code possesses CZ gates between code blocks via the cup product (see below for an introduction), while in Ref. [33], the authors present fold-transversal gates that exist in BB codes. In this section, we introduce an approach to finding CZ gates in multi-block codes, including BB and TT

codes, that is distinct from these previous approaches.

Consider the following depth-1 circuit of CZ gates, where  $\beta \in \mathcal{M}$  is arbitrary:

$$\begin{aligned} \overline{CZ}_{\text{CR},\beta} = \prod_{\alpha \in \mathcal{M}} & CZ[q(C, \alpha), q(R, \beta\alpha^\top)] \\ & CZ[q(R, \alpha), q(C, \beta\alpha^\top)], \end{aligned} \quad (45)$$

where the first (second) argument of  $CZ[\cdot, \cdot]$  refers to a data qubit in the first (second) code block. Similarly to above,  $q(C, \alpha)$  refers to the C data qubit labelled by monomial  $\alpha$ . Let us consider how an  $X$  stabilizer from the first code block is transformed by this circuit:

$$\begin{aligned} \{X(\alpha A, \alpha B, \alpha C)\}_1 \mapsto & \{X(\alpha A, \alpha B, \alpha C)\}_1 \\ & \{Z(0, \beta\alpha^\top C^\top, \beta\alpha^\top B^\top)\}_2, \end{aligned} \quad (46)$$

where we use curly brackets and a subscript to indicate the code block on which the Pauli operator acts. The  $Z$ -type operator is a stabilizer of the second code block: it corresponds to the  $\beta\alpha^\top$ -labelled  $Z_a$ -check. The  $X$  stabilizers of the second code block are similarly transformed. Hence, the above transversal gate preserves the code space. We have two other sets of transversal gates formed in the same way:

$$\begin{aligned} \overline{CZ}_{\text{LR},\beta} = \prod_{\alpha} & CZ[q(L, \alpha), q(R, \beta\alpha^\top)] \\ & CZ[q(R, \alpha), q(L, \beta\alpha^\top)] \end{aligned} \quad (47)$$

$$\begin{aligned} \overline{CZ}_{\text{LC},\beta} = \prod_{\alpha} & CZ[q(L, \alpha), q(C, \beta\alpha^\top)] \\ & CZ[q(C, \alpha), q(L, \beta\alpha^\top)]. \end{aligned} \quad (48)$$

We note that gates of the form  $\overline{CZ}_{\text{LR},\beta}$  are similarly transversal logical gates of BB codes.

If we can find a decomposition of the logicals into three commuting sets (Equations 34–36), then the actions of two of these gates on the logical operators becomes particularly simple. Consider, for example, the  $X$ -logicals from Equation 34 and the gates  $\overline{CZ}_{\text{LC},\beta}$  and  $\overline{CZ}_{\text{CR},\beta}$ :

$$\overline{CZ}_{\text{LC},\beta} : \{\bar{X}_\alpha^{(1)}\}_1 \mapsto \{\bar{X}_\alpha^{(1)}\}_1 \{\bar{Z}_{\beta\alpha^\top}^{(2)}\}_2 \quad (49)$$

$$\{\bar{X}_\alpha^{(2)}\}_1 \mapsto \{\bar{X}_\alpha^{(2)}\}_1 \{\bar{Z}_{\beta\alpha^\top}^{(1)}\}_2$$

$$\{\bar{X}_\alpha^{(3)}\}_1 \mapsto \{\bar{X}_\alpha^{(3)}\}_1;$$

$$\overline{CZ}_{\text{CR},\beta} : \{\bar{X}_\alpha^{(3)}\}_1 \mapsto \{\bar{X}_\alpha^{(3)}\}_1 \{\bar{Z}_{\beta\alpha^\top}^{(2)}\}_2$$

$$\{\bar{X}_\alpha^{(2)}\}_1 \mapsto \{\bar{X}_\alpha^{(2)}\}_1 \{\bar{Z}_{\beta\alpha^\top}^{(3)}\}_2 \quad (50)$$

$$\{\bar{X}_\alpha^{(1)}\}_1 \mapsto \{\bar{X}_\alpha^{(1)}\}_1.$$

The transformation of the  $X$ -logicals from block two is equivalent, owing to the symmetry of the CZ gates. Hence, these gates act as logical  $\overline{CZ}$  gates on certain logical qubits. For example,  $\overline{CZ}_{\text{LC},\beta}$  is a logical  $\overline{CZ}$  between qubit  $\alpha$  in the first set and qubit  $\beta\alpha^\top$  in the second set (for all  $\alpha$ ) in both blocks of code, while acting as the

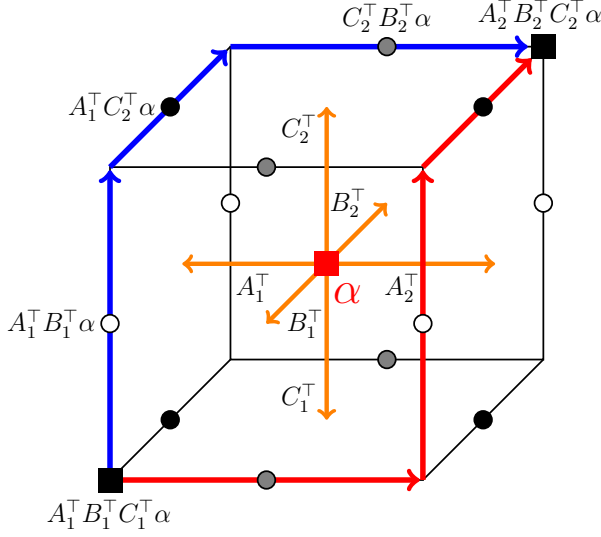


FIG. 6. Prescription for applying  $CCZ$  gates within each cube (labelled by meta-check  $\alpha \in \mathcal{M}$ ) in order to implement a logical non-Clifford gate in a TT code with polynomials  $A = A_1 + A_2$ ,  $B = B_1 + B_2$  and  $C = C_1 + C_2$ . Two example paths that correspond to  $CCZ$  gates are shown in blue and red.

identity on all qubits in the third set. The third type of  $\overline{CZ}$  gate does not have such a simple representation as the above, generically performing some circuit of logical  $CZ$  gates between all logical qubits. We note that TT codes also possess transversal CNOT gates owing to the fact that they are CSS codes. We also note that we numerically observe these  $CZ$  gates to have non-trivial logical action even in the case in which the logical qubits cannot be fully decomposed into one of the sets from Equations 34–36.

### C. Constant-depth $CCZ$ circuits

We finally investigate the possibility of fault-tolerant non-Clifford gates in TT codes. Fault-tolerant logical  $CCZ$  gates have been implemented on certain QLDPC codes using a construction derived from the cohomological cup product [35, 62–64]. This technique has recently been applied to hypergraph product codes and homological products of LDPC codes, showing favourable asymptotic scaling [65, 66].

We show below that any TT code whose checks are based on weight-2 polynomials,  $A = A_1 + A_2$ ,  $B = B_1 + B_2$ , and  $C = C_1 + C_2$ , admits a logical  $\overline{CCZ}$ . Crucially, this gate is implementable via a depth-2 physical  $CCZ$  circuit, similar to what is used for the 3D Toric code on a cubic lattice. We call such a code a (2,2,2) TT code, with the numbers referring to the weights of the polynomials  $A$ ,  $B$  and  $C$ , respectively; we detail this construction in the next section.

To explain the circuit that implements the logical  $\overline{CCZ}$  gate, consider a meta-check labelled by monomial  $\alpha$  (recall the meta-check labelling introduced in Section II B). In the 3D toric code and (2,2,2) TT codes, this corresponds to a cube in the lattice (note this lattice may have highly irregular boundary conditions). A logical gate can be achieved by a constant-depth circuit of  $CCZ$  gates illustrated in Fig. 6 (for all cubes in the lattice). For the cube shown, we first draw an oriented path from  $X$ -check  $A_1^T B_1^T C_1^T \alpha$  to  $X$ -check  $A_2^T B_2^T C_2^T \alpha$  (two examples of such paths are shown in the figure). A  $CCZ$  gate is applied for each arrow between the three qubits it intersects, with the first such qubit being in the first code block, the second being in the second block and the third being in the third. For example, the blue path in Fig. 6 corresponds to the  $CCZ$  gate:

$$CCZ[q(R, A_1^T B_1^T \alpha), q(C, A_1^T C_1^T \alpha), q(L, C_2^T B_2^T \alpha)]. \quad (51)$$

In Table III, we enumerate (2,2,2) codes found by performing exhaustive searches over low dimension sizes,  $\ell$ ,  $m$  and  $p$ . Each of these codes admits a logical  $\overline{CCZ}$  gate. All codes found have  $k = 3$ , which can be understood from the fact that they are equivalent to 3DTCs on a lattice with permuted boundary conditions (see Ref. [15] for an analysis of BB codes on 2D lattices with similarly permuted boundaries). In Table III, we compare the qubit overhead of the corresponding code found to that of the 3DTC with equivalent distance. We also numerically verify that, for all codes found, the  $CCZ$  circuit from Fig. 6 implements a logical transformation of the same form as for the 3DTC. Let us label the three logical qubits of a (2,2,2) TT code  $a$ ,  $b$  and  $c$  respectively. In the following, we will let  $\overline{CCZ}(a, b, c)$  refer to a logical  $CCZ$  gate acting on logical qubit  $a$  from the first code block,  $b$  from the second, and  $c$  from the third. We find that the logical action of the  $CCZ$  circuit is then given by:

$$\begin{aligned} & \overline{CCZ}(a, b, c) \overline{CCZ}(a, c, b) \overline{CCZ}(b, a, c) \\ & \overline{CCZ}(b, c, a) \overline{CCZ}(c, a, b) \overline{CCZ}(c, b, a). \end{aligned} \quad (52)$$

That is, for all codes, the  $CCZ$  circuit implements 6 logical  $\overline{CCZ}$  gates. We compare this with other codes found in the subsequent section.

We note that the  $X$  and  $Z$  distances for the codes found are more balanced than they are for the 3DTC, with  $d_X < d_Z^2$ . The codes presented in Table III were examples of those with the best parameters found after performing an exhaustive search over certain small dimension sizes. We numerically verified that the  $CCZ$  circuit preserves the stabilizer groups of the codes found (see Appendix C).

#### 1. TT Codes with Cup Products

The existence of logical  $\overline{CCZ}$  gates in (2,2,2) TT codes can be understood via the formalism of the cup product

Code parameters	$\frac{n(d)}{n_{TC}(d)}$	$\ell, m, p$	$d_Z, d_X$	Polynomials	No. Logical CCZs
$[[36, 3, 3]]$	4/9	3, 2, 2	3, 8	$A = 1 + xyz, B = 1 + x^2z, C = 1 + x^2y$	6
$[[48, 3, 4]]$	1/4	4, 2, 2	4, 8	$A = 1 + x, B = 1 + xz, C = 1 + xy$	6
$[[54, 3, 4]]$	9/32	3, 3, 2	4, 9	$A = 1 + yz, B = 1 + xz, C = 1 + xyz$	6
$[[60, 3, 4]]$	5/16	5, 2, 2	4, 12	$A = 1 + xz, B = 1 + xy, C = 1 + xyz$	6
$[[90, 3, 5]]$	6/25	5, 3, 2	5, 15	$A = 1 + x, B = 1 + xy, C = 1 + x^2y^2z$	6

TABLE III. Examples of  $(2, 2, 2)$  TT codes with  $CCZ$  gates that have non-trivial logical action. Second column: ratio of  $n$  for the TT code with distance  $d$  to that of the 3D toric code with equivalent distance. Final column: we enumerate the number of logical  $\overline{CCZ}$  gates implemented by the depth-2  $CCZ$  circuit from Fig. 6. Other columns are equivalent to those from Table I.

(see Ref. [35]). Whenever one can define a cup product on a TT code, one can find a constant-depth circuit of  $CCZ$  gates that preserves the stabilizer [35]. Meanwhile, for TT codes, we can define a cup product whenever the polynomials obey certain conditions which we will now outline. We can divide the terms in each polynomial  $A$ ,  $B$  and  $C$  into three sets:  $A = A_{\text{in}} + A_{\text{out}} + A_{\text{free}}$  and similarly for  $B$  and  $C$ . Let us focus on the  $A$  polynomial for now. If we let  $|f|$  denote the number of terms in polynomial  $f$ , and  $|f \cap g|$  denote the number of terms that are shared by polynomials  $f$  and  $g$ , then a cup product exists when the following conditions hold (see Appendix C):

$$|A_{\text{in}}(\alpha_1)| + |A_{\text{out}}(\alpha_1)| = 0 \quad (53)$$

$$|A_{\text{in}}(\alpha_1) \cap A_{\text{in}}(\alpha_2)| = 0 \quad (54)$$

$$|A_{\text{out}}(\alpha_1) \cap A_{\text{out}}(\alpha_2)| + |A_{\text{free}}(\alpha_1) \cap A_{\text{out}}(\alpha_2)| = 0 \quad (55)$$

$$|A_{\text{free}}(\alpha_1) \cap A_{\text{in}}(\alpha_2)| = 0 \quad (56)$$

$$|A(\alpha_1) \cap A_{\text{in}}(\alpha_2) \cap A_{\text{in}}(\alpha_3)| + |A_{\text{out}}(\alpha_1) \cap A(\alpha_2) \cap A_{\text{in}}(\alpha_3)| = 0 \quad (57)$$

for  $\alpha_1$ ,  $\alpha_2$  and  $\alpha_3$  all distinct monomials, and where all addition is done modulo 2. Note these conditions need to be satisfied for  $A$ ,  $B$  and  $C$ .

These conditions can be trivially satisfied by setting  $|A| = |B| = |C| = 2$ , with  $A = A_{\text{in}} + A_{\text{out}}$ , etc. This results in  $(2, 2, 2)$  TT codes, which we discussed above. We also have the following more non-trivial example of polynomials that allow us to define a cup product:  $A_{\text{in}} = A_1 + A_2$ ,  $A_{\text{out}} = A_3 + A_4$  and  $A_{\text{free}} = 0$ , where  $A_1^\top A_2$  and  $A_3^\top A_4$  are equal and self-inverse. This is an example of a more general type of polynomial that satisfies the conditions from Equations 53 – 57. We summarise this with the following:

**Lemma 5.** *A TT code with all three polynomials ( $A$ ,  $B$ , and  $C$ ) either weight-2 or of the form  $P = \sum_{k=1}^{\text{ord}(g)} g^k f$ , where  $g \in \mathcal{M}$  is such that  $\text{ord}(g)$  is even, and  $f$  is an arbitrary (non-zero) polynomial, admits a cup product.*

We prove this Lemma in Appendix C.

We focus on polynomials of the form  $(1 + g)(1 + \alpha)$  with  $g, \alpha \in \mathcal{M}$  and  $g^2 = 1$ , which is the lowest-weight non-trivial polynomial of the form from Lemma 5. We choose  $A$  to be of this form, while  $B$  and  $C$  are chosen to be weight-2 (in Appendix C, we include some examples of codes with one or both of  $B$  and  $C$  also chosen to be weight-4). We refer to these as  $(4, 2, 2)$  codes. The resulting codes have weight-8  $X$ -checks and weight-6 or weight-4  $Z$ -checks. The  $CCZ$  circuit that preserves the stabilizer for such codes is given in Appendix C.

For reasons not fully understood, for all codes found, either the  $CCZ$  gate resulting from the cup product construction has trivial logical action, or the code distance is 2. Note that in the former case, the code distance can be larger than 2. This is the case for all  $(4, 2, 2)$ ,  $(4, 4, 2)$  and  $(4, 4, 4)$  codes found, along with all  $(6, 2, 2)$  codes found (wherein we set  $A$  to have weight 6). However, the full set of minimum-weight logicals for the codes found often includes several that are higher weight than 2. We detail all  $Z$ -logical weights, along with the  $X$ -distance of the codes, in Table IV. For all codes, we test the logical action of the  $CCZ$  circuit, which is always a collection of  $\overline{CCZ}$  logical gates between three code blocks. For any such gate,  $\overline{CCZ}(a, b, c)$ , the distance-2 logical qubit(s) features in one of the code blocks. Hence, gauge fixing this logical qubit results in a trivial logical action. However, the distance-2 logical qubits were not the only ones affected by the  $CCZ$  gates. In Table IV we report the number of logical  $CCZ$  gates applied by the non-Clifford circuit, in the logical basis given by the minimum-weight  $Z$ -logicals from the third column of the table.

We finish this section by commenting that, while the codes in Table IV are only error-detecting (owing to their distance of 2), by gauge-fixing the distance-2 logical qubit, they can result in *error-correcting* codes that have an *additional*  $CZ$  gate, on top of those found in the previous section. We note that the logical  $\overline{CCZ}$  action for the codes found can involve the distance-

2 logical qubit(s) along with two other logical qubits of higher distance. We can form an error-correcting code with an additional  $CZ$  gate as outlined below. For concreteness, we focus on the  $[[36, 6, 2]]$  code from Table IV. Observe that the  $CCZ$  circuit implements (among others) the following logical gates (for one choice of basis with  $Z$ -logical weights given in Table IV):  $\overline{CCZ}(5, 1, 3)\overline{CCZ}(5, 3, 1)\overline{CCZ}(5, 2, 4)\overline{CCZ}(5, 4, 2)$ . In this circuit, logical qubit 5 has  $Z$  logical with minimum-weight 2, while all others have  $Z$  logicals with minimum-weight 3. All other logical gates involve qubit 5 from code blocks 2 and/or 3. The steps to obtain a series of  $\overline{CZ}$  gates on a gauge-fixed code are:

1. Gauge fix the second and third blocks of  $[[36, 6, 2]]$  code so that the distance-2 qubit (qubit 5) is in the  $|0\rangle$  state. This results in a  $[[36, 5, 3]]$  code. Note that this gauge fixing involves measuring  $\bar{Z}_5$ , which commutes with the  $CCZ$  circuit.
2. Consider the gate  $\mathcal{C}_{CCZ}\bar{X}_5 \otimes \bar{1} \otimes \bar{1}\mathcal{C}_{CCZ}$ , where  $\mathcal{C}_{CCZ}$  is the  $CCZ$  circuit obtained from the cup product (given in Appendix C 3), and  $\bar{X}_5 \otimes \bar{1} \otimes \bar{1}$  is the logical  $X$  operator for qubit 5 in the first code block. The logical action of this gate between code blocks 2 and 3 is:  $\overline{CZ}(1, 3)\overline{CZ}(3, 1)\overline{CZ}(2, 4)\overline{CZ}(4, 2)$ .
3. Delete the first code block and truncate circuit  $\mathcal{C}_{CCZ}\bar{X}_5 \otimes \bar{1} \otimes \bar{1}\mathcal{C}_{CCZ}$  to a circuit of  $CZ$ s acting on code blocks 2 and 3.

In this way, one can obtain a larger number of Clifford gates in gauge-fixed versions of the codes from Table IV, which will have higher distances.

## VI. CONCLUSION

In this work, we have investigated a new code construction, the trivariate tricycle codes, which combine several properties useful for future fault-tolerant quantum computation: high thresholds under circuit-level noise, single-shot decodability and fault-tolerant logical gates. The construction includes codes with encoding rates and relative distances that outperform topological codes based on 2D- or 3D-local connectivity. By way of example, our  $[[432, 12, 12]]$  code outperforms the 3D toric code encoding 12 logical qubits at  $d_Z = 12$  by a factor of 48. Furthermore, the  $X$ - and  $Z$ -distances of many codes found are naturally more balanced for the TT codes than they are for the 3DTC, meaning we can obtain the benefits of a 3D code without such a large distance asymmetry. While the code parameters do not reach those attained by bivariate bicycle codes, we note that the inherent distance asymmetry means the  $X$ -distances outperform those of other qLDPC codes (for similar  $n$  and  $k$ ). While the distance asymmetry could be eliminated by distance balancing techniques [67], it could indeed be useful for code platforms that have a biased noise profile,

making either  $Z$  or  $X$  errors more common. Future work could look into distance balancing or further adaptations of the TT codes to biased noise.

The TT codes possess meta-checks in one basis, with a meta-check distance equal to  $d_Z$ . This allows for partial single-shot decodability, which we demonstrate using a circuit-level noise simulation and an overlapping window decoding strategy. We demonstrate the high thresholds and pseudo-thresholds of our codes using the syndrome extraction circuit of Appendix B. The high performance is quite surprising given the large depth of this circuit. We note that this circuit was found analytically and we have not made an attempt to optimise its performance – it is possible that further improvements could be made by attempting to maximise the circuit-level distance. The  $Z$  memory performance of the codes is particularly high, with pseudo-thresholds around 1%. The large meta-check distance also could allow for single-shot generalised lattice-surgery protocols to be performed [28]. Usually, such protocols require  $d$  rounds of measurement, but this could be exchanged for a constant number of measurement rounds. Future work could investigate the spacetime overheads for such protocols using TT codes. It would also be instructive to perform an investigation into any potential single-shot properties of these codes in the  $X$  basis memory experiments.

We investigated several proposals for fault-tolerant Clifford and non-Clifford gates in TT codes. We introduced shift automorphisms and transversal  $CZ$  gates between code blocks, identifying a logical basis in which many of these gates have a simple logical action. And we identified several polynomial constructions that allowed for a constant-depth  $CCZ$  circuit to be defined which preserves the code space. These included all weight-2 polynomials, along with polynomials of the form covered in Lemma 5.

We presented several codes in Table III with logical  $\overline{CCZ}$  gates (over three code blocks) implementable by constant-depth circuits. These codes outperform the regular 3DTC with the same  $Z$ -distance by around a factor of 4, and have lower distance asymmetry than the 3DTC between  $d_Z$  and  $d_X$ . We also present several codes with logical  $\overline{CCZ}$ 's that have better encoding rates but a  $Z$ -distance of only 2 for one or more of the logical qubits.

Here we comment on several avenues for future work relating to non-Clifford gates in TT codes. We have found that, while not all polynomials of the form from Lemma 5 result in codes with distance 2, those that have distance higher than 2 have trivial logical action resulting from the  $CCZ$  circuit presented in Appendix C 3 – it acts as the logical identity. Understanding this feature better and exploring other polynomial constructions that may result in better codes is a crucial avenue for future work.

Despite their limitations, the distance-2 codes could be useful in certain magic state distillation protocols [68–71], because they could allow for higher-fidelity magic states to be created with post-selection, as they can detect er-

Code parameters	$\ell, m, p$	Z-logical weights	$\mathbf{d}_x$	Polynomials	No. Logical CCZs
$[[36, 6, 2]]$	$3, 2, 2$	$3, 3, 3, 3, 3, 2$	$3$	$A = (1+z)(1+x)$ $B = 1+x$ $C = 1+xyz$	$16$
$[[48, 6, 2]]$	$4, 2, 2$	$5, 5, 4, 4, 4, 2$	$4$	$A = (1+x^2yz)(1+xz)$ $B = 1+x^3$ $C = 1+x^3yz$	$10$
$[[54, 9, 2]]$	$3, 3, 2$	$5, 5, 3, 3,$ $3, 3, 3, 2, 2$	$4$	$A = (1+z)(1+y)$ $B = 1+xyz$ $C = 1+x^2y^2$	$36$
$[[108, 6, 2]]$	$4, 3, 3$	$7, 6, 6, 6, 6, 2$	$6$	$A = (1+x^2)(1+xz)$ $B = 1+x^2y^2$ $C = 1+x^2y^2z^2$	$10$
$[[108, 18, 2]]$	$4, 3, 3$	$\{7\} \times 5, \{6\} \times 2,$ $\{2\} \times 11$	$4$	$A = (1+x^2)(1+xy^2z^2)$ $B = 1+x^2y^2z$ $C = 1+x^2y^2z$	$114$

TABLE IV. Examples of (4,2,2) codes with  $CCZ$  gates that have non-trivial logical action. Third column: Rather than simply reporting the  $Z$ -distance (which is 2 in all cases), we report the minimum weights found for all independent  $Z$ -logical operators. Fifth column: The  $A$  polynomial is chosen to have weight-4, and to be of the form  $(1+g)(1+a)$ , where  $g^2 = 1$  and  $a \neq 1$  is arbitrary. Sixth column: Number of logical  $\overline{CCZ}$  gates implemented by the constant-depth circuit of physical  $CCZ$  gates in a basis defined by the  $Z$ -logical operators with weights given in the third column.

rors in one basis and correct errors in the other. There are trade-offs between the number of logical qubits, the level of error-correction that can be performed, and the number of logical  $\overline{CCZ}$  gates that can be implemented (and hence the amount of magic that can be injected into the code space). The way these trade-offs play out in a chosen scheme would influence code selection. This is another avenue for future work. Furthermore, by gauge-fixing the distance-2 logical qubit(s) of these codes, we obtain higher-distance codes with an additional circuit of  $CZ$  gates that has a non-trivial logical action. Future work could explore four-block codes with cup products that could be gauge-fixed in a similar way so that they have non-Clifford logical gates and larger distances.

*Note added:* While this work was being completed, related work appeared in Ref. [72]. There the authors present multi-block constructions for group algebra codes, which include a construction similar to equations 12 – 14. They do not, however, study the trivariate tricycle codes, or their logic gates, presented here.

## VII. ACKNOWLEDGEMENTS

The authors would like to thank Nikolas Breuckmann, Riley Chien, Oscar Higgott, Timo Hillmann, Rebecca Radebold, Tom Scruby, Mackenzie Shaw, and Mark Webster for enlightening discussions. AJ was supported by the Engineering and Physical Sciences Research Council [grant number EP/S021582/1]. CM and DEB were supported by the Engineering and Physical Sciences Research Council [grant number EP/Y004620/1]. CM acknowledges support from the Intelligence Advanced Research Projects Activity (IARPA), under the Entangled Logical Qubits program through Cooperative Agreement Number W911NF-23-2-0223.

## Appendix A: TT code examples, properties, and logical sets

In this Appendix, we present more TT code examples, along with their properties. In Table V, we present several codes obtained by performing a random search

through weight-3 polynomials, setting the first term of each to 1, without loss of generality (see Lemma 3). Along with the code parameters, dimensions, and polynomials, we state whether there exists one of the logical sets from Equations 34–36 that covers all logical qubits in the code. This is based on an exhaustive search through the three logical sets, and through all possible combinations of polynomials  $f$ , and  $[g, h, j]$ , and monomials  $\alpha \in \mathcal{M}$  that feature in each of the logical sets. In the case that we cannot find a logical set that covers all logical qubits, we state the maximum number of logical Pauli  $\bar{X}$  and  $\bar{Z}$  operators that can be covered by a single logical set (i.e., a single choice of  $f$  and  $[g, h, j]$ , and for all choices of  $\alpha \in \mathcal{M}$ ). Note also that, in the cases in which we cannot find a single set that covers all logicals, we still observe that we can cover all logicals by varying  $f$  and  $[g, h, j]$  in the construction of the sets. That is, for each logical Pauli  $\bar{X}$  or  $\bar{Z}$ , there exists a choice of  $f, g, h, j$ , and  $\alpha$  such that the logical operator is of one of the forms in Equations 34–36.

We also state (without proofs, since they are analogous to those found in Ref. [12]) Lemmas relating to the connectivity of the Tanner graphs and 3D-toric layout (see Section II B) of TT codes:

**Lemma 6.** *A TT code based on matrices  $A$ ,  $B$  and  $C$  has a connected Tanner graph if  $\{A_i A_j^\top | i, j \in \{1, 2, 3\}\} \cup \{B_i B_j^\top | i, j \in \{1, 2, 3\}\} \cup \{C_i C_j^\top | i, j \in \{1, 2, 3\}\}$  generate  $\mathcal{M}$ .*

**Lemma 7.** *A TT code based on matrices  $A$ ,  $B$  and  $C$  has a 3D toric layout if there exists  $i, j, g, h, k, o \in \{1, 2, 3\}$  such that:*

- (i)  $\langle A_i A_j^\top, B_g B_h^\top, C_k C_o^\top \rangle = \mathcal{M}$  and
- (ii)  $\text{ord}(A_i A_j^\top) \text{ord}(B_g B_h^\top) \text{ord}(C_k C_o^\top) = \ell_{\text{mp}}$ .

All the TT codes we consider in this paper have connected Tanner graphs but most do not have a 3D toric layout. Some exceptions include the  $[[81, 6, 6]]$  and  $[[648, 12, 14]]$  codes from Table V.

We finally prove Lemma 4, important for the construction of the logical sets, which we repeat here:

**Lemma 4.**  *$X(P, Q, S)$  and  $Z(\bar{P}, \bar{Q}, \bar{S})$  anti-commute if and only if  $1 \in P\bar{P}^\top + Q\bar{Q}^\top + S\bar{S}^\top$ .*

*Proof.* One can write:

$$\begin{aligned} P &= \sum_{\alpha \in \mathcal{M}} p_\alpha \alpha, & \bar{P} &= \sum_{\alpha \in \mathcal{M}} \bar{p}_\alpha \alpha, \\ Q &= \sum_{\alpha \in \mathcal{M}} q_\alpha \alpha, & \bar{Q} &= \sum_{\alpha \in \mathcal{M}} \bar{q}_\alpha \alpha, \\ S &= \sum_{\alpha \in \mathcal{M}} s_\alpha \alpha, & \bar{S} &= \sum_{\alpha \in \mathcal{M}} \bar{s}_\alpha \alpha, \end{aligned} \quad (\text{A1})$$

where  $p_\alpha, \bar{p}_\alpha, q_\alpha, \bar{q}_\alpha, s_\alpha, \bar{s}_\alpha \in \mathbb{F}_2$  are coefficients. Pauli operators  $Z(\bar{P}, \bar{Q}, \bar{S})$  and  $X(P, Q, S)$  overlap on a qubit  $q(L, \alpha)$  iff  $p_\alpha \bar{p}_\alpha = 1$ ,  $q(C, \alpha)$  iff  $q_\alpha \bar{q}_\alpha = 1$  and  $q(R, \alpha)$  iff

$s_\alpha \bar{s}_\alpha = 1$ . This means:

$$\begin{aligned} P\bar{P}^\top &= \sum_{\alpha \in \mathcal{M}} p_\alpha \bar{p}_\alpha 1 + \dots, \\ Q\bar{Q}^\top &= \sum_{\alpha \in \mathcal{M}} q_\alpha \bar{q}_\alpha 1 + \dots, \\ S\bar{S}^\top &= \sum_{\alpha \in \mathcal{M}} s_\alpha \bar{s}_\alpha 1 + \dots, \end{aligned} \quad (\text{A2})$$

By the matrix structure of the monomials the transpose operation is equal to the inverse, and the existence of 1 indicates operators are acting on the same qubit. The dots represent all monomials different from 1, i.e. non-overlap qubits. Then by linearity,

$$P\bar{P} + Q\bar{Q} + S\bar{S} = \sum_{\alpha \in \mathcal{M}} (p_\alpha \bar{p}_\alpha + q_\alpha \bar{q}_\alpha + s_\alpha \bar{s}_\alpha) 1 + \dots \quad (\text{A3})$$

Thus proving the statement.  $\square$

## Appendix B: Syndrome measurement circuits

In this Appendix, we illustrate our syndrome measurement circuits and prove that they perform the required check measurements and preserve the logical operators of the code. The circuit is summarised in Fig. 7. We label blocks of qubits (represented by wires in the figure) by  $X$  (for  $X$ -check measure qubits),  $R$ ,  $C$ ,  $L$  (for the right, center, and left blocks of data qubits),  $Z_a$ ,  $Z_b$  and  $Z_c$  (for the three blocks of  $Z$ -check measure qubits, corresponding to the three blocks of rows in  $H_Z$ ). Each CNOT gate in the diagram represents a collection of CNOT gates, all of which can be performed in parallel, between data and measure qubits in the corresponding blocks (see below).

Note that these circuits have the complication that the  $Z_b$  and  $Z_c$  blocks of measure qubits switch labels every round – this is indicated after the resets in Fig. 7. In order to not introduce an extra idling layer, we omit explicit resets on the  $X$ -measure qubits, instead performing a Pauli frame update dependent on the outcomes of measurements of the  $X$ -measure qubits (alternatively, one could assume having an additional  $n/3$   $X$ -measure qubits available). The lack of resets can be accommodated by updating the definitions of detectors (see, e.g., Ref. [53]). This should not drastically affect quantum memory performance, though it decreases the time-like distance of certain logical operations, like (generalised) lattice surgery (see, e.g., Ref. [53, 54]). For simplicity, in our simulations, we perform a noiseless reset rather than update the definitions of detectors. As drawn, the circuits have depth 13. The first reset in a layer is on the  $Z_a$ -measure qubits and the final measurement is on the  $X$ -measure qubits. If we perform resets on the  $X$ -measure qubits, the circuits become depth-14, however the 2-qubit gate depth remains the same.

The ordering of the matrices in the gates is important and noted in the equations below. We prove that the syn-

$[[n, k, d]]$	$\ell, m, p$	$d_x$	$\mathbf{A}$	$\mathbf{B}$	$\mathbf{C}$	Complete logical sets?
$[[36, 6, 4]]$	$3, 2, 2$	8	$1 + x + x^2z$	$1 + xy + x^2y$	$1 + xyz + x^2$	$\times$ (max. logicals 6)
$[[72, 6, 6]]$	$4, 3, 2$	12	$1 + y + xy^2$	$1 + yz + x^2y^2$	$1 + xy^2z + x^2y$	$\times$ (max. logicals 6)
$[[81, 6, 6]]$	$3, 3, 3$	12	$1 + x + xy$	$1 + y + yz$	$1 + z + x$	$\checkmark$
$[[126, 6, 8]]$	$7, 3, 2$	22	$1 + y^2 + x^4y$	$1 + xy + x^4y^2z$	$1 + x^2yz + x^2y^2$	$\checkmark$
$[[135, 12, 6]]$	$5, 3, 3$	14	$1 + x + x^3y^2$	$1 + xz^2 + x^2yz$	$1 + xy^2z + x^2yz$	$\checkmark$
$[[180, 12, 8]]$	$5, 4, 3$	20	$1 + x^2y^3z + x^4y$	$1 + x^3 + x^4z^2$	$1 + x^3y^3 + x^4yz^2$	$\checkmark$
$[[288, 6, 10]]$	$8, 4, 3$	$\leq 48$	$1 + yz + x^7yz^2$	$1 + x^2yz + x^5z^2$	$1 + x^2y^3z + x^6y^2z^2$	$\times$ (max. logicals 6)
$[[432, 12, 12]]$	$6, 6, 4$	$\leq 36$	$1 + xyz^3 + x^3y^4z^2$	$1 + x^3yz^2 + x^3y^2z^3$	$1 + x^4y^3z^3 + x^5z^2$	$\times$ (max. logicals 12)
$[[588, 9, 14]]$	$7, 7, 4$	$\leq 92$	$1 + yz + x^3y^2z$	$1 + xy^4z + x^4y^4z^2$	$1 + x^2y^2z + x^2y^4$	$\checkmark$
$[[648, 6, 16]]$	$6, 6, 6$	$\leq 72$	$1 + xz^4 + x^3yz^4$	$1 + xy^4z + x^5yz^5$	$1 + x^2yz^2 + x^2y^2z^3$	$\checkmark$
$[[648, 12, 14]]$	$6, 6, 6$	$\leq 72$	$1 + x + x^4z$	$1 + y + xyz^4$	$1 + z + x^3y^2z$	$\times$ (max. logicals 12)
$[[735, 18, 14]]$	$7, 7, 5$	$\leq 80$	$1 + y^2 + x^6y^5$	$1 + x^2yz + x^2y^4z^3$	$1 + x^4y^5z^2 + x^5y$	$\checkmark$
$[[840, 9, 16]]$	$8, 7, 5$	??	$1 + y^3z + xyz^2$	$1 + y^5z + x^3y^4z$	$1 + xy^3z^4 + x^7yz$	$\checkmark$
$[[1029, 18, 16]]$	$7, 7, 7$	??	$1 + y^2z^3 + x^5y^5z$	$1 + x^2y^5z + x^4z^5$	$1 + x^4y^6 + x^5y^4z^6$	$\checkmark$

TABLE V. Example trivariate tricycle codes and their properties. First column: parameters  $[[n, k, d]]$ ; second column: dimensions of  $x$ ,  $y$  and  $z$ , respectively; third column:  $X$ -distance found; fourth - sixth columns: polynomials defining the code; seventh column: we report whether one can find a logical set (see Section V) that covers all logical qubits in the code.

drome measurement circuits perform as required by observing how they update the  $X$  and  $Z$  stabilizer tableaux (see also Ref. [12]). Let us consider the  $X$ -tableau first. We require the syndrome measurement circuit to update this tableau in the following way:

$$\begin{pmatrix} I & 0 & 0 & 0 & 0 & 0 & 0 \\ 0 & A & B & C & 0 & 0 & 0 \end{pmatrix} \rightarrow \begin{pmatrix} I & A & B & C & 0 & 0 & 0 \\ 0 & A & B & C & 0 & 0 & 0 \end{pmatrix} \quad (\text{B1})$$

where the columns of the tableau are labelled  $X$ ,  $L$ ,  $C$ ,  $R$ ,  $Za$ ,  $Zb$ , and  $Zc$ , in order.

For the  $Z$ -tableau, we require the following transformation:

$$\begin{pmatrix} 0 & 0 & 0 & 0 & I & 0 & 0 \\ 0 & 0 & 0 & 0 & 0 & I & 0 \\ 0 & 0 & 0 & 0 & 0 & 0 & I \\ 0 & 0 & C^\top & B^\top & 0 & 0 & 0 \\ 0 & C^\top & 0 & A^\top & 0 & 0 & 0 \\ 0 & B^\top & A^\top & 0 & 0 & 0 & 0 \end{pmatrix} \rightarrow \begin{pmatrix} 0 & 0 & C^\top & B^\top & I & 0 & 0 \\ 0 & C^\top & 0 & A^\top & 0 & I & 0 \\ 0 & B^\top & A^\top & 0 & 0 & 0 & I \\ 0 & 0 & C^\top & B^\top & 0 & 0 & 0 \\ 0 & C^\top & 0 & A^\top & 0 & 0 & 0 \\ 0 & B^\top & A^\top & 0 & 0 & 0 & 0 \end{pmatrix} \quad (\text{B2})$$

where the columns are labelled similarly to above. We show that the circuit below performs both of these transformations.

For the  $X$ -tableau, we will omit the first column since this is unchanged throughout the circuit. The notation  $\text{CX}_{B_1}(R, Za)$  means we perform a CNOT gate between qubit  $i$  in the  $R$  block of data qubits, and  $Za[B_1[i]]$ , in the block of  $Z$  measure qubits, for  $i = 1, \dots, n/3$ , where  $B_1[i] = j$  if and only if row  $i$  and column  $j$  of  $B_1$  is 1.

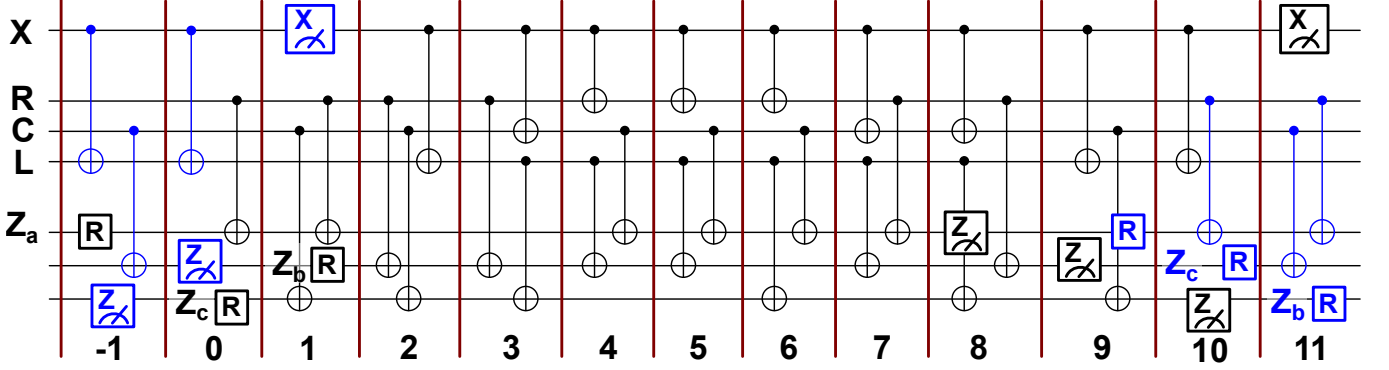


FIG. 7. Syndrome measurement circuit for a trivariate tricycle code, with weight-9  $X$ -checks and weight-6  $Z$ -checks. Gate layers are indicated with numbers below the circuit and delineated with red lines between gates. Lines indicate blocks of data qubits (labelled R, C, and L) or measure qubits (labelled  $X$ ,  $Z_a$ ,  $Z_b$ , or  $Z_c$ ). Blue gates, resets and measurements indicate circuit components from the previous or next syndrome measurement round. The final two qubit lines switch roles between  $Z_b$ - and  $Z_c$ -measure qubits each round, as indicated.

$$\text{Round 0: } \begin{pmatrix} 0 & 0 & 0 & 0 & 0 & 0 \\ A & B & C & 0 & 0 & 0 \end{pmatrix} \xrightarrow{\text{CX}_{B_1}(R, Za)} \begin{pmatrix} 0 & 0 & 0 & 0 & 0 & 0 \\ A & B & C & CB_1 & 0 & 0 \end{pmatrix} \quad (\text{B3})$$

$$\text{Round 1: } \xrightarrow{\substack{\text{CX}_{B_3}(R, Za) \\ \text{CX}_{A_1}(C, Zc)}} \begin{pmatrix} 0 & 0 & 0 & 0 & 0 & 0 \\ A & B & C & C(B_1 + B_3) & 0 & BA_1 \end{pmatrix} \quad (\text{B4})$$

$$\text{Round 2: } \xrightarrow{\substack{\text{CX}_{A_1}(R, Zb) \\ \text{CX}_{A_3}(C, Zc) \\ \text{CX}_{A_2}(X, L)}} \begin{pmatrix} A_2 & 0 & 0 & 0 & 0 & 0 \\ A & B & C & C(B_1 + B_3) & CA_1 & B(A_1 + A_3) \end{pmatrix} \quad (\text{B5})$$

$$\text{Round 3: } \xrightarrow{\substack{\text{CX}_{A_3}(R, Zb) \\ \text{CX}_{B_2}(X, C) \\ \text{CX}_{B_1}(L, Zc)}} \begin{pmatrix} A_2 & B_2 & 0 & 0 & 0 & B_1 A_2 \\ A & B & C & C(B_1 + B_3) & C(A_1 + A_3) & B(A_1 + A_3) + B_1 A \end{pmatrix} \quad (\text{B6})$$

$$\text{Round 4: } \xrightarrow{\substack{\text{CX}_{C_2}(X, R) \\ \text{CX}_{C_1}(C, Za) \\ \text{CX}_{C_1}(L, Zb)}} \begin{pmatrix} A_2 & B_2 & C_2 & C_1 B_2 & C_1 A_2 & B_1 A_2 \\ A & B & C & C(B_1 + B_3) + C_1 B & C(A_1 + A_3) + C_1 A & B(A_1 + A_3) + B_1 A \end{pmatrix} \quad (\text{B7})$$

$$\text{Round 5: } \xrightarrow{\substack{\text{CX}_{C_1}(X, R) \\ \text{CX}_{C_2}(C, Za) \\ \text{CX}_{C_2}(L, Zb)}} \begin{pmatrix} A_2 & B_2 & C_1 + C_2 & (C_1 + C_2) B_2 & (C_1 + C_2) A_2 & B_1 A_2 \\ A & B & C & CB_2 + C_3 B & CA_2 + C_3 A & B(A_1 + A_3) + B_1 A \end{pmatrix} \quad (\text{B8})$$

$$\text{Round 6: } \xrightarrow{\substack{\text{CX}_{C_3}(X, R) \\ \text{CX}_{C_3}(C, Za) \\ \text{CX}_{B_2}(L, Zc)}} \begin{pmatrix} A_2 & B_2 & C & CB_2 & (C_1 + C_2) A_2 & (B_1 + B_2) A_2 \\ A & B & C & CB_2 & CA_2 + C_3 A & BA_2 + B_3 A \end{pmatrix} \quad (\text{B9})$$

$$\text{Round 7: } \xrightarrow{\substack{\text{CX}_{B_2}(R, Za) \\ \text{CX}_{B_1}(X, C) \\ \text{CX}_{C_3}(L, Zb)}} \begin{pmatrix} A_2 & B_1 + B_2 & C & 0 & CA_2 & (B_1 + B_2) A_2 \\ A & B & C & 0 & CA_2 & BA_2 + B_3 A \end{pmatrix} \quad (\text{B10})$$

$$\text{Round 8: } \xrightarrow{\substack{\text{CX}_{A_2}(R, Zb) \\ \text{CX}_{B_3}(X, C) \\ \text{CX}_{B_3}(L, Zc)}} \begin{pmatrix} A_2 & B & C & 0 & 0 & BA_2 \\ A & B & C & 0 & 0 & BA_2 \end{pmatrix} \quad (\text{B11})$$

$$\text{Round 9: } \xrightarrow{\substack{\text{CX}_{A_2}(C, Zc) \\ \text{CX}_{A_1}(X, L)}} \begin{pmatrix} A_1 + A_2 & B & C & 0 & 0 & 0 \\ A & B & C & 0 & 0 & 0 \end{pmatrix} \quad (\text{B12})$$

$$\text{Round 10: } \xrightarrow{\text{CX}_{A_3}(X, L)} \begin{pmatrix} A & B & C & 0 & 0 & 0 \\ A & B & C & 0 & 0 & 0 \end{pmatrix} \quad (\text{B13})$$

The  $Z$ -tableau works similarly. We will omit the last three columns since they are unchanged throughout the circuit.

$$\text{Round 0: } \begin{pmatrix} 0 & 0 & 0 & 0 \\ 0 & 0 & 0 & 0 \\ 0 & 0 & 0 & 0 \\ 0 & 0 & C^\top & B^\top \\ 0 & C^\top & 0 & A^\top \\ 0 & B^\top & A^\top & 0 \end{pmatrix} \xrightarrow{\text{CX}_{B_1}(R, Za)} \begin{pmatrix} 0 & 0 & 0 & B_1^\top \\ 0 & 0 & 0 & 0 \\ 0 & 0 & 0 & 0 \\ 0 & 0 & C^\top & B^\top \\ 0 & C^\top & 0 & A^\top \\ 0 & B^\top & A^\top & 0 \end{pmatrix} \quad (\text{B14})$$

$$\text{Round 1: } \frac{\text{CX}_{B_3}(R, Za)}{\text{CX}_{A_1}(C, Zc)} \begin{pmatrix} 0 & 0 & 0 & B_1^\top + B_3^\top \\ 0 & 0 & 0 & 0 \\ 0 & 0 & A_1^\top & 0 \\ 0 & 0 & C^\top & B^\top \\ 0 & C^\top & 0 & A^\top \\ 0 & B^\top & A^\top & 0 \end{pmatrix} \quad (\text{B15})$$

$$\text{Round 2: } \frac{\text{CX}_{A_1}(R, Zb)}{\text{CX}_{A_3}(C, Zc)} \frac{\text{CX}_{A_2}(X, L)}{\begin{pmatrix} 0 & 0 & 0 & B_1^\top + B_3^\top \\ 0 & 0 & 0 & A_1^\top \\ 0 & 0 & A_1^\top + A_3^\top & 0 \\ 0 & 0 & C^\top & B^\top \\ A_2^\top C^\top & C^\top & 0 & A^\top \\ A_2^\top B^\top & B^\top & A^\top & 0 \end{pmatrix}} \quad (\text{B16})$$

$$\text{Round 3: } \frac{\text{CX}_{A_3}(R, Zb)}{\text{CX}_{B_2}(X, C)} \frac{\text{CX}_{B_1}(L, Zc)}{\begin{pmatrix} 0 & 0 & 0 & B_1^\top + B_3^\top \\ 0 & 0 & 0 & A_1^\top + A_3^\top \\ B_2^\top (A_1^\top + A_3^\top) & B_1^\top & A_1^\top + A_3^\top & 0 \\ B_2^\top C^\top & 0 & C^\top & B^\top \\ A_2^\top C^\top & C^\top & 0 & A^\top \\ A_2^\top B^\top + A^\top B_2^\top & B^\top & A^\top & 0 \end{pmatrix}} \quad (\text{B17})$$

$$\text{Round 4: } \frac{\text{CX}_{C_2}(X, R)}{\text{CX}_{C_1}(C, Za)} \frac{\text{CX}_{C_1}(L, Zb)}{\begin{pmatrix} C_2^\top (B_1^\top + B_3^\top) & 0 & C_1^\top & B_1^\top + B_3^\top \\ C_2^\top (A_1^\top + A_3^\top) & C_1^\top & 0 & A_1^\top + A_3^\top \\ B_2^\top (A_1^\top + A_3^\top) & B_1^\top & A_1^\top + A_3^\top & 0 \\ B_2^\top C^\top + B^\top C_2^\top & 0 & C^\top & B^\top \\ A_2^\top C^\top + A^\top C_2^\top & C^\top & 0 & A^\top \\ A_2^\top B^\top + A^\top B_2^\top & B^\top & A^\top & 0 \end{pmatrix}} \quad (\text{B18})$$

$$\text{Round 5: } \frac{\text{CX}_{C_1}(X, R)}{\text{CX}_{C_2}(C, Za)} \frac{\text{CX}_{C_2}(L, Zb)}{\begin{pmatrix} (C_1^\top + C_2^\top)(B_1^\top + B_3^\top) & 0 & C_1^\top + C_2^\top & B_1^\top + B_3^\top \\ (C_1^\top + C_2^\top)(A_1^\top + A_3^\top) & C_1^\top + C_2^\top & 0 & A_1^\top + A_3^\top \\ B_2^\top (A_1^\top + A_3^\top) & B_1^\top & A_1^\top + A_3^\top & 0 \\ B_2^\top C^\top + B^\top (C_1^\top + C_2^\top) & 0 & C^\top & B^\top \\ A_2^\top C^\top + A^\top (C_1^\top + C_2^\top) & C^\top & 0 & A^\top \\ A_2^\top B^\top + A^\top B_2^\top & B^\top & A^\top & 0 \end{pmatrix}} \quad (\text{B19})$$

$$\text{Round 6: } \frac{\text{CX}_{C_3}(X, R)}{\text{CX}_{C_2}(C, Za)} \frac{\text{CX}_{B_2}(L, Zc)}{\begin{pmatrix} C^\top (B_1^\top + B_3^\top) & 0 & C^\top & B_1^\top + B_3^\top \\ C^\top (A_1^\top + A_3^\top) & C_1^\top + C_2^\top & 0 & A_1^\top + A_3^\top \\ B_2^\top (A_1^\top + A_3^\top) & B_1^\top + B_2^\top & A_1^\top + A_3^\top & 0 \\ B_2^\top C^\top + B^\top C_1^\top & 0 & C^\top & B^\top \\ (A_1^\top + A_3^\top) C^\top & C^\top & 0 & A^\top \\ A_2^\top B^\top + A^\top B_2^\top & B^\top & A^\top & 0 \end{pmatrix}} \quad (\text{B20})$$

$$\text{Round 7: } \xrightarrow{\substack{\text{CX}_{B_2}(R, Za) \\ \text{CX}_{B_1}(X, C) \\ \text{CX}_{C_3}(L, Zb)}} \begin{pmatrix} C^\top B_3^\top & 0 & C^\top & B^\top \\ C^\top(A_1^\top + A_3^\top) & C^\top & 0 & A_1^\top + A_3^\top \\ (B_1^\top + B_2^\top)(A_1^\top + A_3^\top) & B_1^\top + B_2^\top & A_1^\top + A_3^\top & 0 \\ B_3^\top C^\top & 0 & C^\top & B^\top \\ (A_1^\top + A_3^\top)C^\top & C^\top & 0 & A^\top \\ A_2^\top B^\top + A^\top(B_1^\top + B_2^\top) & B^\top & A^\top & 0 \end{pmatrix} \quad (\text{B21})$$

$$\text{Round 8: } \xrightarrow{\substack{\text{CX}_{A_2}(R, Zb) \\ \text{CX}_{B_3}(X, C) \\ \text{CX}_{B_3}(L, Zc)}} \begin{pmatrix} 0 & 0 & C^\top & B^\top \\ C^\top(A_1^\top + A_3^\top) & C^\top & 0 & A^\top \\ B^\top(A_1^\top + A_3^\top) & B^\top & A_1^\top + A_3^\top & 0 \\ 0 & 0 & C^\top & B^\top \\ (A_1^\top + A_3^\top)C^\top & C^\top & 0 & A^\top \\ (A_1^\top + A_3^\top)B^\top & B^\top & A^\top & 0 \end{pmatrix} \quad (\text{B22})$$

$$\text{Round 9: } \xrightarrow{\substack{\text{CX}_{A_2}(C, Zc) \\ \text{CX}_{A_1}(X, L)}} \begin{pmatrix} 0 & 0 & C^\top & B^\top \\ C^\top A_3^\top & C^\top & 0 & A^\top \\ B^\top A_3^\top & B^\top & A^\top & 0 \\ 0 & 0 & C^\top & B^\top \\ A_3^\top C^\top & C^\top & 0 & A^\top \\ A_3^\top B^\top & B^\top & A^\top & 0 \end{pmatrix} \quad (\text{B23})$$

$$\text{Round 10: } \xrightarrow{\text{CX}_{A_3}(X, L)} \begin{pmatrix} 0 & 0 & C^\top & B^\top \\ 0 & C^\top & 0 & A^\top \\ 0 & B^\top & A^\top & 0 \\ 0 & 0 & C^\top & B^\top \\ 0 & C^\top & 0 & A^\top \\ 0 & B^\top & A^\top & 0 \end{pmatrix} \quad (\text{B24})$$

Now let us consider the logical operators. We will consider a  $Z$ -logical first. As in Ref. [12], we write this as  $(u, w, v)$  with  $u$ ,  $w$  and  $v$  restrictions of the operator to the  $L$ ,  $C$  and  $R$  qubits, respectively. The commutation of  $(u, w, v)$  with the  $X$  parity check matrix means:

$$[A \ B \ C] \begin{bmatrix} u \\ w \\ v \end{bmatrix} = Au + Bw + Cv = 0. \quad (\text{B25})$$

Meanwhile, let us consider the action of the SM circuit on the logical. Since this logical has  $Z$  support, the CNOT gates controlled on data qubits have no action on the logical operator. Only the CNOTs targeted on data qubits have action; these are those involved in the  $X$ -check measurements. The support of the updated logical on the  $X$ -measurement qubits is given by:

$$t = Au + Bw + Cv = 0. \quad (\text{B26})$$

For an  $X$  logical operator,  $(u, w, v)$ , the vectors obey:

$$C^\top w + B^\top v = C^\top u + A^\top v = B^\top u + A^\top w = 0. \quad (\text{B27})$$

The supports of the logical on qubits  $Z_a$ ,  $Z_b$  and  $Z_c$  are given by  $t_a$ ,  $t_b$  and  $t_c$  respectively:

$$t_a = (C_1^\top + C_2^\top + C_3^\top)w + (B_1^\top + B_2^\top + B_3^\top)v = 0 \quad (\text{B28})$$

$$t_b = C^\top u + A^\top v = 0 \quad (\text{B29})$$

$$t_c = B^\top u + A^\top w = 0. \quad (\text{B30})$$

Therefore the logical operators are preserved by the circuit.

## Appendix C: Details of logical $CCZ$ gates

### 1. Review of Cup Product Conditions

Here we review some of the ingredients entering into the cup product construction of Ref. [35], from which we derive the non-Clifford gates acting on  $(4,2,2)$  codes and others in this paper.

Consider a classical group algebra code, for abelian  $G$ :

$$C^0 \xrightarrow{A} C^1, \quad (\text{C1})$$

where  $C^0 = C^1 = \mathbb{F}_2[G]$ . Here,  $\mathbb{F}_2[G]$  denotes the formal sums of the form  $\sum_{g \in G} a_g g$ , for  $a_g \in \{0, 1\}$ , and  $A$  is an element of  $\mathbb{F}_2[G]$ . For our purposes, we can assume  $G = \mathbb{Z}_\ell \times \mathbb{Z}_m \times \mathbb{Z}_p$  and  $A$  is a polynomial in the generators of the cyclic subgroups of  $G$ , as is appropriate for a TT code.

We define a *pre-orientation* on this code by partitioning the terms of  $A$  into three disjoint sets:  $A = A_{\text{in}} + A_{\text{out}} + A_{\text{free}}$ . Let  $X_0$  and  $X_1$  represent bases for  $C^0$ , the checks (on which  $A$  acts), and  $C^1$ , the physical bits of the code, respectively. We then define the cup product, a bi-linear map on the chain complex, via:  $\alpha \cup \alpha = \alpha$  for  $\alpha \in X_0$ ;  $\alpha \cup \beta = \beta$  for  $\alpha \in X_0$  and  $\beta \in A_{\text{out}}\alpha$ ;  $\beta \cup \alpha = \beta$  for  $\alpha \in X_0$ ,  $\beta \in A_{\text{in}}\alpha$ ; zero on all other basis inputs. We furthermore define the integral on  $C^1$  to be  $\int_1 f = |f|$  (mod 2), for  $f \in C^1$ . The integrated Leibniz rule for the 3-fold cup product states that for all  $\alpha_i \in C^0$ :

$$\begin{aligned} \int_1 (A\alpha_1 \cup \alpha_2) \cup \alpha_3 + (\alpha_1 \cup A\alpha_2) \cup \alpha_3 \\ + (\alpha_1 \cup \alpha_2) \cup A\alpha_3 = 0 \pmod{2}. \end{aligned} \quad (\text{C2})$$

Note that the multi-fold cup product is not necessarily associative, and hence we retain brackets in the above expression. Not all choices of pre-orientation obey this rule, but it is crucial to being able to define a cohomology operation (and hence a logical gate) from the (balanced) product of two or more of these classical codes.

By using the properties of the cup product, we can write the integrated Leibniz rule as:

$$\begin{aligned} |A\alpha_1 \cap A_{\text{in}}\alpha_2 \cap A_{\text{in}}\alpha_3| + |A_{\text{out}}\alpha_1 \cap A\alpha_2 \cap A_{\text{in}}\alpha_3| \\ + \delta_{\alpha_1, \alpha_2} |A_{\text{out}}\alpha_2 \cap A\alpha_3| = 0 \pmod{2}, \end{aligned} \quad (\text{C3})$$

where  $\delta_{\alpha_1, \alpha_2} = 1$  if  $\alpha_1 = \alpha_2$ , and is zero otherwise.

We now consider when the integrated Leibniz rule is satisfied. First let  $\alpha_1 = \alpha_2 = \alpha_3$ . Then the first term in Equation C3 is simply  $|A_{\text{in}}\alpha_1|$ , the second term is zero and the final term is  $|A_{\text{out}}\alpha_1|$ . This reproduces the condition Equation 53. Now suppose  $\alpha_1 = \alpha_3 \neq \alpha_2$ . Only the first term is potentially non-zero, and we find:

$$|A_{\text{in}}\alpha_1 \cap A_{\text{in}}\alpha_2| = 0 \pmod{2}. \quad (\text{C4})$$

Now suppose  $\alpha_1 = \alpha_2 \neq \alpha_3$ . We find, using Equation C4:

$$\begin{aligned} |A_{\text{out}}\alpha_2 \cap A_{\text{in}}\alpha_3| + |A_{\text{out}}\alpha_2 \cap A\alpha_3| \\ = |A_{\text{out}}\alpha_2 \cap A_{\text{free}}\alpha_3| + |A_{\text{out}}\alpha_2 \cap A_{\text{out}}\alpha_3| \end{aligned} \quad (\text{C5})$$

$$= 0 \pmod{2}. \quad (\text{C6})$$

If  $\alpha_1 \neq \alpha_2 = \alpha_3$  we have:

$$\begin{aligned} |A\alpha_1 \cap A_{\text{in}}\alpha_2| + |A_{\text{out}}\alpha_1 \cap A_{\text{in}}\alpha_2| \\ = |A_{\text{free}}\alpha_2 \cap A_{\text{in}}\alpha_3| = 0 \pmod{2}. \end{aligned} \quad (\text{C7})$$

Finally, if all  $\alpha_i$  are distinct, we have:

$$\begin{aligned} |A\alpha_1 \cap A_{\text{in}}\alpha_2 \cap A_{\text{in}}\alpha_3| + |A_{\text{out}}\alpha_1 \cap A\alpha_2 \cap A_{\text{in}}\alpha_3| \\ = 0 \pmod{2}. \end{aligned} \quad (\text{C8})$$

We therefore obtain all conditions from Equations 54–57.

The formulas for the cup product of the balanced product of three group algebra codes can be found in Ref. [35]. However, we point out that it is only non-zero for inputs of the form:  $\alpha_L \cup \beta_C \cup \gamma_R$  (or for other permutations of the three data qubit blocks). For our purposes, only the form of the *CCZ* circuits implementing the logical non-Clifford gate will be important. We introduce these below.

## 2. Proof of Lemma 5

We now prove Lemma 5, which we restate here:

**Lemma 5.** *A TT code with all three polynomials ( $A$ ,  $B$ , and  $C$ ) either weight-2 or of the form  $P = \sum_{k=1}^{\text{ord } g} g^k f$ , where  $g \in \mathcal{M}$  is such that  $\text{ord } g$  is even, and  $f$  is an arbitrary (non-zero) polynomial, admits a cup product.*

*Proof.* It suffices to show that the polynomials of weight 2 or of the form of  $P$  satisfy the cup product conditions, since  $A$ ,  $B$  and  $C$  must satisfy these conditions individually. To see that a weight-2 polynomial,  $P_1 + P_2$ , satisfies the conditions, simply let  $P_{\text{in}} := P_1$  and  $P_{\text{out}} := P_2$ . All conditions are thereby easily verified.

Let  $G = \sum_{k=1}^{\text{ord } g} g^k$ . We first divide the terms of  $f$  into in, out and free terms:  $f = f_{\text{in}} + f_{\text{out}} + f_{\text{free}}$ . If  $|f| = 1$ , then  $P$  is weight-2, so let us assume  $|f| \geq 2$ . We will choose  $\lfloor |f|/2 \rfloor$  terms to belong to  $f_{\text{in}}$ , arbitrarily, and  $\lfloor |f|/2 \rfloor$  terms to belong to  $f_{\text{out}}$ , with any remaining term belonging to  $f_{\text{free}}$ . Note that this is not a unique choice. We will then choose  $P_{\text{in}} = Gf_{\text{in}} \equiv G(f_{\text{in}}^{(1)} + f_{\text{in}}^{(2)} + \dots)$ , and similarly for  $P_{\text{out}}$  and  $P_{\text{free}}$ . The fact that  $\text{ord } g$  is even ensures that  $|P_{\text{in}}\alpha| = |P_{\text{out}}\alpha| \pmod{2}$ .

We begin by showing that  $|Gh_1\alpha \cap Gh_2\beta| = 0 \pmod{2}$  when  $\alpha \neq \beta$ , where  $h_1$  and  $h_2$  are arbitrary polynomials. Let us suppose that  $Gh_1 \cap Gh_2 \neq \emptyset$ , so that  $g^k h_1^{(i)} \alpha = g^l h_2^{(j)} \beta$ , for some integers  $k, l, i, j$ , where  $h_1^{(i)}$  is the  $i^{\text{th}}$  term in  $h_1$ , etc. But this implies the following relations also hold:

$$\begin{aligned} g^{k+1} h_1^{(i)} \alpha &= g^{l+1} h_2^{(j)} \beta \\ g^{k+2} h_1^{(i)} \alpha &= g^{l+2} h_2^{(j)} \beta \\ &\dots \\ g^{k+\text{ord } g-1} h_1^{(i)} \alpha &= g^{l+\text{ord } g-1} h_2^{(j)} \beta. \end{aligned}$$

Since  $\text{ord } g$  is even, and all the above are distinct, there are an even number of such relations. If we can find another relation,  $g^{k'} h_1^{(i')} \alpha = g^{l'} h_2^{(j')} \beta$ , this will produce a set of relations either distinct from the above entirely, or it will reproduce the set of above relations. This is because, if we reproduce one of the above relations, then  $g^{k+M} h_1^{(i)} \alpha = g^{l+M} h_2^{(j)} \beta = g^{k'} h_1^{(i')} \alpha = g^{l'} h_2^{(j')} \beta$ , for some integer  $M$ , and it is easy to see that all relations will be reproduced. We conclude therefore,  $|Gh_1\alpha \cap Gh_2\beta| = K \text{ord } g = 0 \pmod{2}$ , where  $K$  is an integer.

From the above, we conclude that  $|P_{\text{in}}\alpha \cap P_{\text{in}}\beta| = |P_{\text{in}}\alpha \cap P_{\text{free}}\beta| = |P_{\text{out}}\alpha \cap P_{\text{out}}\beta| = |P_{\text{free}}\alpha \cap P_{\text{out}}\beta| = 0 \pmod{2}$ , for  $\alpha \neq \beta$ . To show that Equation 57 holds, we note that  $P_{\text{in}}\alpha_2 \cap P_{\text{in}}\alpha_3 = Gh$ , for some (potentially zero) polynomial  $h$ , and similarly for  $P_{\text{out}} \cap P_{\text{out}}$  and  $P_{\text{in}} \cap P_{\text{free}}$ . We can use this, along with the above, to show that Equation 57 holds.  $\square$

### 3. Circuit implementing logical non-Clifford gates

We now explain the constant-depth  $CCZ$  circuit that preserves the stabilizer for codes that admit a cup product. We apply the following gates to the data qubits:

$$\prod_{\substack{\alpha \in \mathcal{M}, \\ \beta \in \mathcal{Q}_{2,\text{out}} \mathcal{Q}_{1,\text{in}}^\top \alpha, \\ \gamma \in \mathcal{Q}_{3,\text{out}} \mathcal{Q}_{2,\text{in}}^\top \beta}} CCZ(q(Q_1, \alpha), q(Q_2, \beta), q(Q_3, \gamma)) \quad (\text{C9})$$

for all choices of data qubit blocks  $Q_1, Q_2, Q_3$ , which are all distinct elements from  $\{\text{L, C, R}\}$ . In the above, we use  $\mathcal{Q}_i$  to refer to the polynomial from block  $Q_i$  in  $H_X$ . I.e., if  $Q_i = \text{L}$ ,  $\mathcal{Q}_i = A$ , if  $Q_i = \text{C}$ ,  $\mathcal{Q}_i = B$ , and if  $Q_i = \text{R}$ ,  $\mathcal{Q}_i = C$ .

### 4. Details of numerics used to find logical action of $CCZ$ circuits

Here, we detail the methods used to obtain the results from Section V C. For each code with a non-trivial  $CCZ$  circuit, we make an assignment of terms in  $A, B$  and  $C$  into in, out and free subsets, as detailed above. We then build a description of the  $CCZ$  circuit from Equation C9: for each gate in the circuit, we include in the circuit description a tuple of the form  $(q_1, q_2, q_3)$ , for row vectors  $q_i$  corresponding to qubits in the support of the gate, and where the three slots of the tuple correspond to the three blocks of code. Then for every pair of  $X$ -checks in different code blocks, we check that the  $CCZ$

circuit maps their product to a  $Z$ -stabilizer of the final code block. We describe this procedure in Algorithm 1.

The intuition for the algorithm is that it checks whether the  $CCZ$  circuit conjugates  $X$ -stabilizers in any two code blocks to a  $Z$ -stabilizer in the third block. We note in the algorithm that  $\text{rows}(A)$  corresponds to the set of rows of matrix  $A$ , while  $\text{rs}(A)$  corresponds to the row space of  $A$  (i.e., the span of all rows of  $A$  over the field  $\mathbb{F}_2$ ). We also note that it suffices to pick one stabilizer (labelled  $\text{row}_1$  in Algorithm 1) of the first code block arbitrarily before looping over only the second-code-block  $X$ -stabilizer ( $\text{row}_2$ ). This is because all other first-block  $X$ -stabilizers are related to  $\text{row}_1$  by a monomial. This monomial can be absorbed into the product over  $\alpha \in \mathcal{M}$  in the circuit (Equation C9) and hence if the circuit conjugates  $\text{row}_1$  and  $\text{row}_2$  to a  $Z$ -stabilizer (for all choices of  $\text{row}_2$ ) it does so for all choices of  $\text{row}_1$ . This is simply a result of the translation invariance of the code.

We next check which logical qubits are acted upon non-trivially by the logical gate implemented by the  $CCZ$  circuit. We begin by producing a minimum-weight set of  $Z$ -logicals,  $L_Z$ , whose weights are given in Table IV, using the QDistRnd algorithm [45]. We then produce a set of  $X$ -logicals,  $L_X$ , that are conjugate to those minimum-weight  $Z$ -logicals:  $L_X L_Z^\top = \mathbb{1}_k$ . We then determine the logical action of the  $CCZ$  circuit on this set of  $X$ -logicals by determining the “intersection number” for each triple of logicals, which counts the number of  $CCZ$  gates in circuit C9 that intersect  $l_1$  in code block 1,  $l_2$  in block 2 and  $l_3$  in block 3. If and only if this intersection number  $I(l_1, l_2, l_3) = 1 \pmod{2}$ , the  $CCZ$  circuit implements the logical gate  $CCZ(l_1, l_2, l_3)$  between the three code blocks. We enumerate the number of logical triples that produce a non-trivial intersection number in Tables III, IV, and VI. We verify that a non-trivial intersection number is obtained only if one of the logicals  $l_i$  is conjugate to a weight-2  $Z$ -logical.

### Appendix D: (4,4,2) and (4,4,4) code examples

In Table VI, we detail just two examples of codes with two or three polynomials set to have weight-4 (and of the form from Lemma 5). These codes all admit a cup product and hence a constant-depth circuit of the form given in Equation C9 which acts non-trivially on the code space. The codes listed have many weight-2  $Z$ -logicals and very large numbers of logical  $CCZ$  gates enacted by the circuit of physical  $CCZ$ s. These particular codes are also found to have weight-2  $X$ -logicals.

---

[1] S. B. Bravyi and A. Y. Kitaev, Quantum codes on a lattice with boundary (1998), arXiv:quant-ph/9811052 [quant-ph].

[2] E. Dennis, A. Kitaev, A. Landahl, and J. Preskill, Topological Quantum Memory, Journal of Mathematical Physics **43**, 4452 (2002).

---

**Algorithm 1:** Check  $CCZ$  Circuit Preserves Code's Stabilizer Group

---

**Input:** Matrices  $H_X, H_Z$ ; List of  $CCZ$  gates in circuit C9,  $L$  (each is a length-3 tuple of qubit indices corresponding to the support of that gate in the three code blocks)

**Output:** **true** if  $CCZ$  circuit is valid, **false** otherwise

Initialize **result**  $\leftarrow$  **true**;

for  $i$  in  $(1, 2, 3)$  and  $j$  in  $(1, 2, 3)$  such that  $i \neq j$  do

$\text{row}_1 \leftarrow$  First row of  $H_X$ ;

$\text{Ind}(\text{row}_1) \leftarrow$  List of indices corresponding to non-zero elements of  $\text{row}_1$ ;

$n \leftarrow$  number of columns in  $H_X$ ;

for each  $\text{row}_2$  in  $\text{rows}(H_X)$  do

$\text{Ind}(\text{row}_2) \leftarrow$  List of indices corresponding to non-zero elements of  $\text{row}_2$ ;

$Z\text{-stabilizer candidate} \leftarrow$  row vector of zeros with length  $n$ ;

for each  $qubit_1$  in  $\text{Ind}(\text{row}_1)$  and  $qubit_2$  in  $\text{Ind}(\text{row}_2)$  do

if  $qubit_1$  and  $qubit_2$  are in support of the same  $CCZ$  gate  $G \in L$ , with  $qubit_1$  ( $qubit_2$ ) in the  $i^{th}$  ( $j^{th}$ ) argument of  $G$  then

$qubitvec \leftarrow$  row vector of length  $n$  with 1 in the column corresponding to the qubit in the  $k^{th}$  argument of  $G$  (where  $k \neq i, k \neq j$ ), and zeros in all other columns;

$Z\text{-stabilizer candidate} \leftarrow Z\text{-stabilizer candidate} + qubitvec$ ;

if  $Z\text{-stabilizer candidate}$  is not in  $rs(H_Z)$  then

$\text{result} \leftarrow$  **false**;

return **result**;

return **result**;

---

- [3] A. Kitaev, Fault-tolerant quantum computation by anyons, *Annals of Physics* **303**, 2–30 (2003).
- [4] A. G. Fowler, M. Mariantoni, J. M. Martinis, and A. N. Cleland, Surface codes: Towards practical large-scale quantum computation, *Physical Review A* **86**, 10.1103/physreva.86.032324 (2012).
- [5] D. Litinski, A game of surface codes: Large-scale quantum computing with lattice surgery, *Quantum* **3**, 128 (2019).
- [6] D. Horsman, A. G. Fowler, S. Devitt, and R. V. Meter, Surface code quantum computing by lattice surgery, *New Journal of Physics* **14**, 123011 (2012).
- [7] C. Gidney, Inplace access to the surface code y basis, *Quantum* **8**, 1310 (2024).
- [8] B. J. Brown, K. Laubscher, M. S. Kesselring, and J. R. Wootton, Poking holes and cutting corners to achieve

clifford gates with the surface code, *Physical Review X* **7**, 10.1103/physrevx.7.021029 (2017).

- [9] C. Gidney, N. Shutty, and C. Jones, Magic state cultivation: growing t states as cheap as cnot gates (2024), arXiv:2409.17595 [quant-ph].
- [10] C. Gidney, M. Newman, P. Brooks, and C. Jones, Yoked surface codes (2023), arXiv:2312.04522 [quant-ph].
- [11] M. E. Beverland, P. Murali, M. Troyer, K. M. Svore, T. Hoefler, V. Kliuchnikov, G. H. Low, M. Soeken, A. Sundaram, and A. Vaschillo, Assessing requirements to scale to practical quantum advantage (2022), arXiv:2211.07629 [quant-ph].
- [12] S. Bravyi, A. W. Cross, J. M. Gambetta, D. Maslov, P. Rall, and T. J. Yoder, High-Threshold and Low-Overhead Fault-Tolerant Quantum Memory, *Nature* **627**, 778 (2024).
- [13] T. J. Yoder, E. Schoute, P. Rall, E. Pritchett, J. M. Gambetta, A. W. Cross, M. Carroll, and M. E. Beverland, Tour de gross: A modular quantum computer based on bivariate bicycle codes (2025), arXiv:2506.03094 [quant-ph].
- [14] A. A. Kovalev and L. P. Pryadko, Quantum kronecker sum-product low-density parity-check codes with finite rate, *Phys. Rev. A* **88**, 012311 (2013).
- [15] L. Voss, S. J. Xian, T. Haug, and K. Bharti, Multivariate bicycle codes (2025), arXiv:2406.19151 [quant-ph].
- [16] M. Wang and F. Mueller, Coprime bivariate bicycle codes (2024), arXiv:2408.10001 [quant-ph].
- [17] H.-K. Lin and L. P. Pryadko, Quantum two-block group algebra codes (2023), arXiv:2306.16400 [quant-ph].
- [18] Z. Liang, K. Liu, H. Song, and Y.-A. Chen, Generalized toric codes on twisted tori for quantum error correction (2025), arXiv:2503.03827 [quant-ph].
- [19] Z. Liang, J. N. Eberhardt, and Y.-A. Chen, Planar quantum low-density parity-check codes with open boundaries (2025), arXiv:2504.08887 [quant-ph].
- [20] M. Ye and N. Delfosse, Quantum error correction for long chains of trapped ions (2025), arXiv:2503.22071 [quant-ph].
- [21] K. Wang, Z. Lu, C. Zhang, G. Liu, J. Chen, Y. Wang, Y. Wu, S. Xu, X. Zhu, F. Jin, Y. Gao, Z. Tan, Z. Cui, N. Wang, Y. Zou, A. Zhang, T. Li, F. Shen, J. Zhong, Z. Bao, Z. Zhu, Y. Han, Y. He, J. Shen, H. Wang, J.-N. Yang, Z. Song, J. Deng, H. Dong, Z.-Z. Sun, W. Li, Q. Ye, S. Jiang, Y. Ma, P.-X. Shen, P. Zhang, H. Li, Q. Guo, Z. Wang, C. Song, H. Wang, and D.-L. Deng, Demonstration of low-overhead quantum error correction codes (2025), arXiv:2505.09684 [quant-ph].
- [22] E. T. Campbell, A theory of single-shot error correction for adversarial noise, *Quantum Science and Technology* **4**, 025006 (2019).
- [23] A. O. Quintavalle, M. Vasmer, J. Roffe, and E. T. Campbell, Single-shot error correction of three-dimensional homological product codes, *PRX Quantum* **2**, 020340 (2021).
- [24] O. Higgott and N. P. Breuckmann, Improved single-shot decoding of higher-dimensional hypergraph-product codes, *PRX Quantum* **4**, 10.1103/prxquantum.4.020332 (2023).
- [25] T. R. Scruby, T. Hillmann, and J. Roffe, High-threshold, low-overhead and single-shot decodable fault-tolerant quantum memory (2024), arXiv:2406.14445 [quant-ph].
- [26] H.-K. Lin, X. Liu, P. K. Lim, and L. P. Pryadko, Single-shot and two-shot decoding with generalized bi-

Code parameters	$\ell, m, p$	Z-logical weights	X-logical weights	Polynomials	No. Logical CCZs
$[[108, 18, 2]]$	$4, 3, 3$	$\{7\} \times 5, \{6\} \times 2, \{2\} \times 11$	$\{13\} \times 5, \{6\} \times 8 \{2\} \times 5$	$A = (1 + x^2)(1 + xyz^2)$ $B = (1 + x^2)(1 + x^3y^2z)$ $C = 1 + x^2y^2z^2$	204
$[[108, 60, 2]]$	$4, 3, 3$	$\{5\} \times 2, \{4\} \times 8, \{3\} \times 10, \{2\} \times 40,$	$\{9\} \times 2, \{6\} \times 14, \{3\} \times 6, \{2\} \times 38,$	$A = (1 + x^2)(1 + z)$ $B = (1 + x^2)(1 + x^2yz^2)$ $C = (1 + x^2)(1 + z^2)$	552

TABLE VI. Examples of (4,4,2) and (4,4,4) codes with CCZ gates with non-trivial logical action.

cycle codes (2025), arXiv:2502.19406 [quant-ph].

[27] Y. Hong, Single-shot preparation of hypergraph product codes via dimension jump (2024), arXiv:2410.05171 [quant-ph].

[28] T. Hillmann, G. Dauphinais, I. Tzitrin, and M. Vasmer, Single-shot and measurement-based quantum error correction via fault complexes (2024), arXiv:2410.12963 [quant-ph].

[29] A. Kubica and M. E. Beverland, Universal transversal gates with color codes: A simplified approach, *Physical Review A* **91**, 10.1103/physreva.91.032330 (2015).

[30] N. P. Breuckmann and S. Burton, Fold-transversal Clifford Gates for Quantum Codes, *Quantum* **8**, 1372 (2024).

[31] A. O. Quintavalle, P. Webster, and M. Vasmer, Partitioning qubits in hypergraph product codes to implement logical gates, *Quantum* **7**, 1153 (2023).

[32] A. J. Malcolm, A. N. Glaudell, P. Fuentes, D. Chandra, A. Schotte, C. DeLisle, R. Haenel, A. Ebrahimi, J. Roffe, A. O. Quintavalle, S. J. Beale, N. R. Lee-Hone, and S. Simmons, Computing efficiently in qldpc codes (2025), arXiv:2502.07150 [quant-ph].

[33] J. N. Eberhardt and V. Steffan, Logical operators and fold-transversal gates of bivariate bicycle codes (2024), arXiv:2407.03973 [quant-ph].

[34] H. Sayginel, S. Koutsoumpas, M. Webster, A. Rajput, and D. E. Browne, Fault-tolerant logical clifford gates from code automorphisms (2025), arXiv:2409.18175 [quant-ph].

[35] N. P. Breuckmann, M. Davydova, J. N. Eberhardt, and N. Tantivasadakarn, Cups and gates I: Cohomology invariants and logical quantum operations (2024), arXiv:2410.16250 [quant-ph].

[36] T.-C. Lin, Transversal non-clifford gates for quantum ldpc codes on sheaves (2024), arXiv:2410.14631 [quant-ph].

[37] L. Golowich and T.-C. Lin, Quantum ldpc codes with transversal non-clifford gates via products of algebraic codes (2024), arXiv:2410.14662 [quant-ph].

[38] Q. T. Nguyen, Good binary quantum codes with transversal ccz gate (2024), arXiv:2408.10140 [quant-ph].

[39] Z. He, A. Cowtan, D. J. Williamson, and T. J. Yoder, Extractors: Qldpc architectures for efficient pauli-based computation (2025), arXiv:2503.10390 [quant-ph].

[40] L. Daguerre and I. H. Kim, Code switching revisited: Low-overhead magic state preparation using color codes, *Physical Review Research* **7**, 10.1103/physrevresearch.7.023080 (2025).

[41] A. Wills, M.-H. Hsieh, and H. Yamasaki, Constant-overhead magic state distillation (2024), arXiv:2408.07764 [quant-ph].

[42] D. Ruiz, J. Guillaud, A. Leverrier, M. Mirrahimi, and C. Vuillot, Ldpc-cat codes for low-overhead quantum computing in 2d, *Nature Communications* **16**, 10.1038/s41467-025-56298-8 (2025).

[43] P. Panteleev and G. Kalachev, Asymptotically Good Quantum and Locally Testable Classical LDPC Codes, in *Proceedings of the 54th Annual ACM SIGACT Symposium on Theory of Computing* (2022) pp. 375–388.

[44] N. P. Breuckmann and J. N. Eberhardt, Balanced product quantum codes, *IEEE Transactions on Information Theory* **67**, 6653–6674 (2021).

[45] L. P. Pryadko, V. A. Shabashov, and V. K. Kozin, Qdis-trnd: A gap package for computing the distance of quantum error-correcting codes, *Journal of Open Source Software* **7**, 4120 (2022).

[46] M. Webster, CSSLO (2024), original-date: 2022-12-14T23:54:25Z.

[47] J. Roffe, LDPC: Python tools for low density parity check codes (2022).

[48] C. Gidney, Stim: a fast stabilizer circuit simulator, *Quantum* **5** (2021).

[49] J. Roffe, D. R. White, S. Burton, and E. Campbell, Decoding across the quantum low-density parity-check code landscape, *Physical Review Research* **2**, 10.1103/physrevresearch.2.043423 (2020).

[50] L. Skoric, D. E. Browne, K. M. Barnes, N. I. Gillespie, and E. T. Campbell, Parallel window decoding enables scalable fault tolerant quantum computation, *Nature Communications* **14**, 10.1038/s41467-023-42482-1 (2023).

[51] X. Tan, F. Zhang, R. Chao, Y. Shi, and J. Chen, Scalable surface-code decoders with parallelization in time, *PRX Quantum* **4**, 040344 (2023).

[52] B. J. Brown, N. H. Nickerson, and D. E. Browne, Fault-tolerant error correction with the gauge color code, *Nature Communications* **7**, 10.1038/ncomms12302 (2016).

- [53] G. P. Gehér, M. Jastrzebski, E. T. Campbell, and O. Crawford, To reset, or not to reset – that is the question (2025), arXiv:2408.00758 [quant-ph].
- [54] R. Harper, C. Lainé, E. Hockings, C. McLauchlan, G. M. Nixon, B. J. Brown, and S. D. Bartlett, Characterising the failure mechanisms of error-corrected quantum logic gates (2025), arXiv:2504.07258 [quant-ph].
- [55] P. Virtanen, R. Gommers, T. E. Oliphant, M. Haberland, T. Reddy, D. Cournapeau, E. Burovski, P. Peterson, W. Weckesser, J. Bright, S. J. van der Walt, M. Brett, J. Wilson, K. J. Millman, N. Mayorov, A. R. J. Nelson, E. Jones, R. Kern, E. Larson, C. J. Carey, I. Polat, Y. Feng, E. W. Moore, J. VanderPlas, D. Laxalde, J. Perktold, R. Cimrman, I. Henriksen, E. A. Quintero, C. R. Harris, A. M. Archibald, A. H. Ribeiro, F. Pedregosa, P. van Mulbregt, and SciPy 1.0 Contributors, SciPy 1.0: Fundamental Algorithms for Scientific Computing in Python, *Nature Methods* **17**, 261 (2020).
- [56] P.-J. H. Derkx, A. Townsend-Teague, A. G. Burchards, and J. Eisert, Designing fault-tolerant circuits using detector error models, arXiv preprint arXiv:2407.13826 (2024).
- [57] O. Higgott, STIMBPOSD: An implementation of the BP+OSD decoder for circuit-level noise. (2024).
- [58] J. S. Yedidia, W. T. Freeman, Y. Weiss, *et al.*, Understanding belief propagation and its generalizations, Exploring artificial intelligence in the new millennium **8**, 0018 (2003).
- [59] Z. Babar, P. Botsinis, D. Alanis, S. X. Ng, and L. Hanzo, Fifteen years of quantum ldpc coding and improved decoding strategies, *IEEE Access* **3**, 2492 (2015).
- [60] S. Koutsoumpas, H. Sayginel, M. Webster, and D. E. Browne, Automorphism ensemble decoding of quantum ldpc codes, arXiv preprint arXiv:2503.01738 (2025).
- [61] L. A. Beni, O. Higgott, and N. Shutty, Tesseract: A search-based decoder for quantum error correction, arXiv preprint arXiv:2503.10988 (2025).
- [62] G. Zhu, S. Sikander, E. Portnoy, A. W. Cross, and B. J. Brown, Non-clifford and parallelizable fault-tolerant logical gates on constant and almost-constant rate homological quantum ldpc codes via higher symmetries (2024), arXiv:2310.16982 [quant-ph].
- [63] Y.-A. Chen and S. Tata, Higher cup products on hypercubic lattices: Application to lattice models of topological phases, *Journal of Mathematical Physics* **64**, 10.1063/5.0095189 (2023).
- [64] Y. Wang, Y. Wang, Y.-A. Chen, W. Zhang, T. Zhang, J. Hu, W. Chen, Y. Gu, and Z.-W. Liu, Efficient fault-tolerant implementations of non-clifford gates with reconfigurable atom arrays, *npj Quantum Information* **10**, 10.1038/s41534-024-00945-3 (2024).
- [65] G. Zhu, A topological theory for qldpc: non-clifford gates and magic state fountain on homological product codes with constant rate and beyond the  $N^{1/3}$  distance barrier, arXiv preprint arXiv:2501.19375 (2025).
- [66] G. Zhu, Transversal non-clifford gates on qldpc codes breaking the  $\sqrt{N}$  distance barrier and quantum-inspired geometry with  $\mathbb{Z}_2$  systolic freedom, arXiv preprint arXiv:2507.15056 (2025).
- [67] M. B. Hastings, Weight reduction for quantum codes (2016), arXiv:1611.03790 [quant-ph].
- [68] S. Bravyi and A. Kitaev, Universal quantum computation with ideal clifford gates and noisy ancillas, *Physical Review A* **71**, 10.1103/physreva.71.022316 (2005).
- [69] S. Bravyi and J. Haah, Magic-state distillation with low overhead, *Physical Review A* **86**, 10.1103/physreva.86.052329 (2012).
- [70] D. Litinski, Magic state distillation: Not as costly as you think, *Quantum* **3**, 205 (2019).
- [71] P. Sales Rodriguez *et al.*, Experimental demonstration of logical magic state distillation, *Nature* 10.1038/s41586-025-09367-3 (2025).
- [72] H.-K. Lin, P. K. Lim, A. A. Kovalev, and L. P. Pryadko, Abelian multi-cycle codes for single-shot error correction (2025), arXiv:2506.16910 [quant-ph].